The periodic topography of ice stream beds: insights from the Fourier spectra of mega-scale glacial lineations

Matteo Spagnolo[1,2], Timothy C. Bartholomaus[3], Chris D. Clark[4], Chris R. Stokes[5], Nigel Atkinson[6], Julian A. Dowdeswell[7], Jeremy C. Ely[4], Ali G.C. Graham[8], Kelly A. Hogan[9], Edward C. King[9], Robert D. Larter[9], Stephen J. Livingstone[4], Hamish D. Pritchard[9]

1. Department of Geography and the Environment, School of Geosciences, University of Aberdeen, UK
2. Department of Earth and Planetary Science, University of California at Berkeley, USA
3. Department of Geological Sciences, University of Idaho, Moscow, Idaho, USA
4. Department of Geography, University of Sheffield, UK
5. Department of Geography, Durham University, UK
6. Alberta Geological Survey, Canada
7. Scott Polar Research Institute, University of Cambridge, UK
8. Department of Geography, University of Exeter, UK
9. British Antarctic Survey, UK

KEY POINTS

1. MSGL topography consists of superimposed periodic wavelengths as expected in the instability theory of subglacial bedform formation
2. Most of the dominant wavelengths present within one extensive MSGL field increase downstream suggesting MSGLs evolve via pattern coarsening
3. For MSGLs to generate periodic topography sediment must be able to accumulate or erode (freely move) without fixed anchor points

ABSTRACT

Ice stream bed topography contains key evidence for the ways ice streams interact with, and are potentially controlled by, their beds. Here we present the first application of two–dimensional Fourier analysis to 22 marine and terrestrial topographies from 5 regions in Antarctica and Canada, with and without mega-scale glacial lineations (MSGLs). We find that the topography of MSGL-rich ice stream sedimentary beds is characterized by multiple, periodic wavelengths between 300 and 1200 m and amplitudes from decimeters to a few meters. This periodic topography is consistent with the idea that instability is a key element to the formation of MSGL bedforms. Dominant wavelengths vary among locations and, on one paleo ice stream bed, increase along the direction of ice flow by 1.7±0.52% km^{-1}. We suggest that these changes are likely to reflect pattern evolution via downstream wavelength coarsening, even under potentially steady ice stream geometry and flow conditions. The amplitude of MSGLs is smaller than that of other fluvial and glacial topographies, but within the same order of magnitude. However, MSGLs are a striking component of ice stream beds because the topographic amplitude of features not aligned with ice flow is reduced by an order of magnitude relative to those oriented with the flow direction. This study represents the first attempt to automatically derive the spectral signatures of MSGLs. It highlights the plausibility of identifying these landform

assemblages using automated techniques and provides a benchmark for numerical models of ice stream flow and subglacial landscape evolution.

Keywords: ice stream, mega-scale glacial lineations, subglacial bedforms, spectral analysis, pattern formation

1. INTRODUCTION

Mega-scale glacial lineations (MSGLs) are elongated sedimentary ridges of low relief and represent the landform signature of fast-flowing ice streams [e.g. *Clark, 1994; Canals et al., 2000; Stokes and Clark, 2001; Ó Cofaigh et al., 2002; King et al., 2009*]. Ice streams are the primary drainage routes for much of the ice flowing to the ocean from the Antarctic and Greenland Ice Sheets, as they were for the Pleistocene ice sheets [*Bamber et al., 2000; Bennett, 2003; Rignot and Kanagaratnam, 2006; Rignot et al., 2011*]. Ice stream dynamics influence ice sheet mass balance, and play a fundamental role in regulating sea level changes [*Anderson et al., 2002; Stokes et al., 2016*]. Ice stream flow is known to be influenced by both external and internal forcing mechanisms [e.g. *Bindschadler et al., 2003; Jamieson et al., 2014; Fisher et al., 2015*], but is ultimately controlled by the interaction between fast-flowing ice and the bed, where MSGLs are formed [e.g. *Engelhardt et al., 1990; Joughin et al., 2004; Piotrowski et al., 2004*]. The genesis and evolution of these landforms can therefore reveal key clues about the processes occurring at the ice-bed interface and on the mechanism(s) of ice stream flow [e.g. *Jamieson et al., 2016; Spagnolo et al., 2016*]. Although the beds of modern ice streams provide important information [e.g. *Smith et al., 2007; King et al., 2009*], unimpeded access to paleo-ice stream beds in both terrestrial and marine settings can shed light on ice stream behaviors and processes that took place over longer time-scales than modern observations permit [e.g. *Beget, 1986, Hicock et al., 1989; Dowdeswell et al., 2004; Ó Cofaigh et al., 2005; Stokes and Clark, 2001; Margold et al., 2015a*]. Despite the importance of this topic and the multiple hypotheses proposed, there is presently no consensus on the formation of MSGLs [*Lemke, 1958; Bluemle et al., 1993; Clark, 1993; Clark et al., 2003; Shaw et al., 2008; Fowler, 2010; Stokes et al., 2013; Spagnolo et al., 2014*]. Through further investigation of these landforms, existing theories can be tested and new theories inspired, thus providing novel insight into the processes acting at the ice-bed interface. One aspect of MSGL formation that has received relatively little quantitative attention is the spatial organization of ice stream bed topography.

MSGLs are typically defined by their morphology, characterized by parallel ridges and troughs that are kilometers-long, 100s of meters-wide, and only a few meters-high [*Clark, 1993; Spagnolo et al., 2014*]. Despite their similarity to, and spatial association with, other streamlined subglacial bedforms, especially drumlins [*Ely et al., 2016*], a distinctive aspect of MSGLs is that they can occupy entire ice stream beds, without any discernible topographic break between individual landforms. This, and their generally very low (few-meters) amplitude, can make it difficult to identify and delimit individual MSGLs [*Spagnolo et al., 2014*]. Whereas the lack of a topographical break between adjacent MSGLs is evident in ice stream bed topography (Fig. 1), the extent to which MSGLs are spatially organized (i.e. regular) remains unclear. Spatial organization can have important implications for hypotheses of their formation [*Barchyn et al., 2016*], with some predicting that MSGLs evolve via the amplification of initial perturbations that leads to a topography characterized by dominant wavelengths [*Fowler, 2010; Fowler and Chapwanya, 2014*].

A combination of manual and semi-automated geographic information system techniques has recently highlighted that MSGLs in different settings are characterized by similar ridge-to-ridge (across-flow) spacing [*Spagnolo et al., 2014*]. However, that analysis relied on (inevitably subjective) manual mapping and semi-automated measurements, and primarily focused on average values at the scale of a whole ice stream bed. A more robust and objective analysis of the subglacial topography has not yet been achieved, limiting our ability to quantitatively test hypotheses regarding MSGL formation and, more generally, to characterize the interface between ice streams and their beds. At regional scales, studies of ice sheet basal topographies in Antarctica have indicated that ice stream beds have low roughness values that are consistent with a depositional environment and the presence of streamlined bedforms [*Bingham and Siegert, 2009; Li et al., 2010; Rippin et al., 2014*]. However, most previous studies were based on one-dimensional analysis of individual radio-echo sounding profiles of coarse spatial resolution, and only examined wavelengths larger than typical MSGLs. Characterizing the potential regularity of MSGLs, along with their shape and scale, could therefore contribute to the interpretation of ice stream basal roughness and its parameterization in ice sheet models [*Schoof, 2002*].

In this paper, we apply two-dimensional (2D) discrete Fourier transforms to describe the orientation-related roughness of MSGLs and associated topography. We apply the technique to marine and terrestrial locations, and to both modern and paleo-ice stream beds in Antarctica and Canada, to quantitatively address the following questions:

1. Is the topographic signal of MSGLs in the frequency domain distinct from other topographies?
2. To what extent are MSGLs periodic, and do their dominant wavelengths vary from setting to setting or along the length of a single ice stream bed?

The answers to these questions bear directly on theories for the formation and evolution of MSGLs, and the quantitative, spectral analysis presented here allows differentiation among sites that has not been possible using existing methods. Furthermore, characteristic frequency domain signals can serve as input data or output constraints on numerical models of ice stream flow and landscape evolution. Quantification of MSGL spatial regularity and related amplitudes informs our understanding of the low basal roughness beneath ice streams and could prove useful in methods for the automated identification of MSGLs. These results and their implication for ice stream processes are presented and discussed below.

2. METHODS

Unlike traditional mapping techniques, which divide landscapes into discrete entities or landforms, the methodology adopted in this work analyzes the whole topography simultaneously to identify the wavelength and amplitude of periodic features (i.e., waves or ripples across the topography) without the need to manually delineate them. Our approach is to calculate 2D Fourier spectra of glaciated topography in order to derive topographic amplitudes as functions of both orientation and wavelength. Across these 2D spectra, we extract 1D profiles representing periodic topography at a full range of orientations. Because topographic amplitude is typically correlated with wavelength [*Sayles and Thomas, 1978*] and we seek to identify anomalously large-amplitude features, we calculate the median topographic amplitude from all orientations. Amplitudes at each orientation are then normalized by the median amplitude to find the dominant orientations and wavelengths; i.e. those characterized by relatively high-amplitude periodic variations. Our approach enables us to identify and quantitatively characterize the topographic signals with the most regular wave-like expressions.

2.1 Landform datasets

To analyze and compare topographic patterns as functions of wavelength and amplitude (i.e., spectra), we compiled 22, 10 x 10 km digital topographic models (DTMs)

from 5 environmental settings, including the seafloor of formerly glaciated continental shelves [*Ó Cofaigh et al., 2002; Dowdeswell et al., 2004, b; Larter et al., 2009; Anderson and Jakobsson, 2010; Jakobsson et al. 2011; Livingstone et al., 2013, 2016a, 2016b*] and terrestrial landscapes [*Atkinson et al., 2014; Margold et al., 2015a,b*] as well as one modern ice stream bed [*King et al., 2016*]. Half of these areas contain MSGLs. Areas with other distinctive landforms, selected for comparative purposes (Fig. 1 and Tab.1), include: (i) iceberg furrows [e.g. *Woodworth-Lynas et al., 1991*]; (ii) glacially streamlined bedrock; (iii) crag-and-tail features [e.g. *Dowdeswell et al., 2016*]; (iv) shelf-break gullies [e.g. *Gales et al., 2013*]; and (v) terrestrial fluvial landscapes (Fig. 1 and Tab. 1). The source DTMs were derived from LIDARmulti-beam echo-sounding bathymetric surveys, LIDAR scans, or ice-penetrating radio-echo sounding techniques, thus producing outputs of varying resolutions (Tab. 1).

2.2 Calculation of Fourier transforms

Following customary procedures for spectral analysis, each sample DTM was detrended by removing a best-fit plane from the topography before applying a 2D raised cosine (Hann) window as a weighting function to the entire 100 km^2 DTM [*Perron et al., 2008*]. Detrending prevents spurious long-period spectral peaks that would arise through the assumption that finite topographic samples are periodic (an assumption intrinsic to the Fourier transform). Windowing the data maintains sharp spectral resolution (the ability to resolve features with different wavelengths) and minimizes spectral leakage (the smearing of high-amplitude peaks into adjacent frequencies that arises from using discretely-sampled data to characterize continuous topography). Detrending with a plane, rather than a higher-order polynomial, allows us to analyze all topographic wavelengths, without making subjective judgements regarding the removal of low-frequency topographic variations. The result of these steps is a map of elevation deviations from 0 m (via detrending) that smoothly tapers at the edges to 0 m (via windowing; Fig. 2c).

Two-dimensional fast Fourier transforms were then performed on the detrended and 2D Hann-windowed DTMs prior to application of a scalar correction factor to the Fourier transform amplitudes to account for the reduction of amplitudes associated with windowing the data. Finally, resulting spectra were shifted to center the zero frequency and, because the frequency space is 180° rotationally-symmetric for the real-valued DTMs, we discarded their

bottom halves. Figure 3 illustrates an example of the result of these steps for DTM PI_MSGL_1, showing the mean amplitude (half-height) of features with specified easting and northing spatial frequencies. A different reading of these results is to consider them in polar, rather than Cartesian coordinates. In this view, the amplitude with f_x easting and f_y northing frequencies is equivalent to the amplitude of a periodic feature with wavelength

$$\lambda = 1/\sqrt{f_x^2 + f_y^2}$$

and periodic topography oriented at

$$\theta = \tan^{-1}(-f_y/f_x).$$

As defined, θ is the orientation along the crests of corrugations such as MSGL crests and troughs, measured clockwise from north. This definition allows us to describe the strike of the MSGLs and the ice-flow direction, in contrast with the traditional approach of defining orientation as amplitude and wavelength perpendicular to periodic crests. Furthermore, while the wavelengths identified through 1D Fourier transforms depend on the angle between MSGL crests and extracted topographic profiles, the wavelength and amplitude of our 2D analysis are robust to the orientation of the reference frame. In 1D, a same MSGL field will be characterized by longer wavelengths as the angle with the profiles depart from 90°. In 2D, if the two orthogonal axes (initially northing and easting) are rotated over an MSGL field, the periodic frequency of one axis will increase as that of the second axis decreases, such that λ is independent of the reference frame orientation. Thus, in 2D, periodic features return a frequency signal along their specific orientation only (Fig. S1).

192

Region	Resolution		Name	Figure	Setting	Activity	Morphology	Area	Mid point		Dominant	Dominant	Max normalized
	horizontal	vertical						km^2	latitude	longitude	orientation (°)	wavelength (m)	amplitude
Amundsen Sea Embayment, Antarctica	30 m	2 m	ASE_bedrock_1	1a	marine	paleo	streamlined bedrock	100	73.618 S	115.276 W	30.2	1327	8
Amundsen Sea Embayment, Antarctica	30 m	2 m	ASE_bedrock_2	1a	marine	paleo	crag and tails	100	73.524 S	115.202 W	22.6	282	5
Amundsen Sea Embayment, Antarctica	30 m	2 m	ASE_MSGL_1	1a	marine	paleo	MSGLs	100	73.430 S	115.230 W	-13	1188	14
Amundsen Sea Embayment, Antarctica	30 m	2 m	ASE_MSGL_2	1a	marine	paleo	MSGLs	100	73.335 S	115.254 W	-16.2	332	15
Amundsen Sea Embayment, Antarctica	30 m	2 m	ASE_MSGL_3	1a	marine	paleo	MSGLs	100	73.241 S	115.321 W	-30.8	600	13
Pine Island, Antarctica	20 m	1 m	PI_furrows	1b	marine	paleo	iceberg furrows	100	72.929 S	107.152 W	-11.6	1992	4
Pine Island, Antarctica	20 m	1 m	PI_MSGL_1	1b	marine	paleo	MSGLs	100	73.264 S	107.015 W	-12.6	689	42
Pine Island, Antarctica	20 m	1 m	PI_MSGL_2	1b	marine	paleo	MSGLs	100	72.743 S	107.207 W	-18.4	348	34
Lower Athabasca region, Alberta, Canada	2 m	0.1 m	LAR_MSGL	1c	terrestrial	paleo	MSGLs	100	57.865 N	111.989 W	55.8	1626	4
Lower Athabasca region, Alberta, Canada	2 m	0.1 m	LAR_fluvial	1c	terrestrial	paleo	fluvial landscape	100	57.887 N	112.179 W	-86.2	1973	2
Lower Athabasca region, Alberta, Canada	2 m	0.1 m	LAR_flat	1c	terrestrial	paleo	fluvial terrace	100	57.833 N	111.692 W	33.8	1992	2
Marguerite Trough, Antarctica	15 m	1 m	MT_gullies	1d	marine	paleo	shelf break gullies	100	66.551 S	71.694 W	119.8	763	6
Marguerite Trough, Antarctica	15 m	1 m	MT_furrows	1d	marine	paleo	iceberg furrows	100	66.486 S	71.276 W	148.4	1992	4
Marguerite Trough, Antarctica	15 m	1 m	MT_MSGL_1	1d	marine	paleo	MSGLs	100	66.735 S	70.662 W	142	749	17
Marguerite Trough, Antarctica	15 m	1 m	MT_MSGL_2	1d	marine	paleo	MSGLs	100	66.535 S	70.964 W	131.4	317	11
Marguerite Trough, Antarctica	15 m	1 m	MT_MSGL_3	1d	marine	paleo	MSGLs	100	66.866 S	70.860 W	128.6	791	7
Marguerite Trough, Antarctica	15 m	1 m	MT_bedrock_1	1f	marine	paleo	bedrock	100	68.696 S	69.638 W	105.6	1232	6
Marguerite Trough, Antarctica	15 m	1 m	MT_bedrock_2	1f	marine	paleo	bedrock	100	67.965 S	70.340 W	15.4	1390	7
Marguerite Trough, Antarctica	15 m	1 m	MT_bedrock_3	1f	marine	paleo	bedrock	100	68.248 S	69.920 W	3	943	6
Rutford Ice Stream, Antarctica	7.5-500 m	3 m	RIS_MSGL_1	1e	marine	current	MSGLs	100	78.425 S	84.048 W	158	329	N/A
Rutford Ice Stream, Antarctica	7.5-500 m	3 m	RIS_MSGL_2	1e	marine	current	MSGLs	100	78.523 S	83.774 W	160	504	N/A
Rutford Ice Stream, Antarctica	7.5-500 m	3 m	RIS_MSGL_3	1e	marine	current	MSGLs	100	78.619 S	83.496 W	159.8	361	N/A

Table 1. Summary table with details relative to each analyzed DTM.

Formatted: Numbering: Continuous

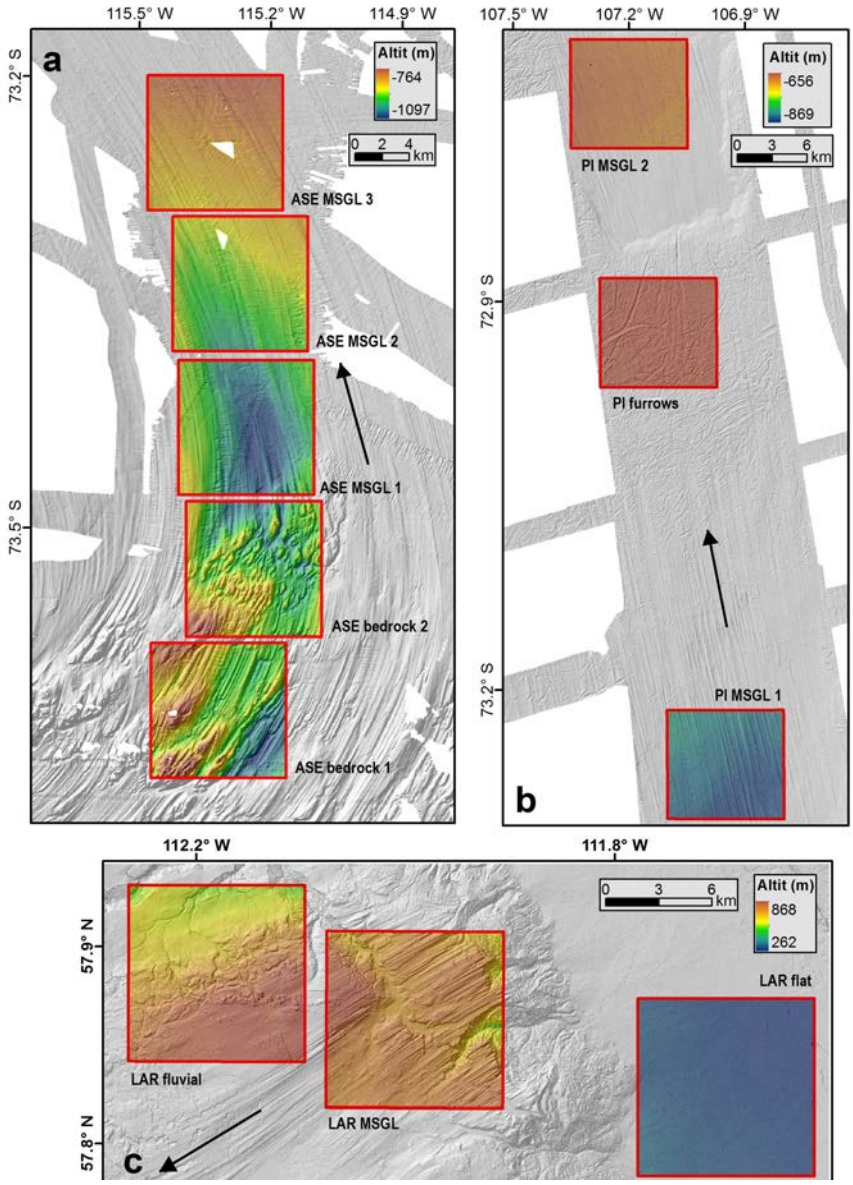

195

Formatted: Numbering: Continuous

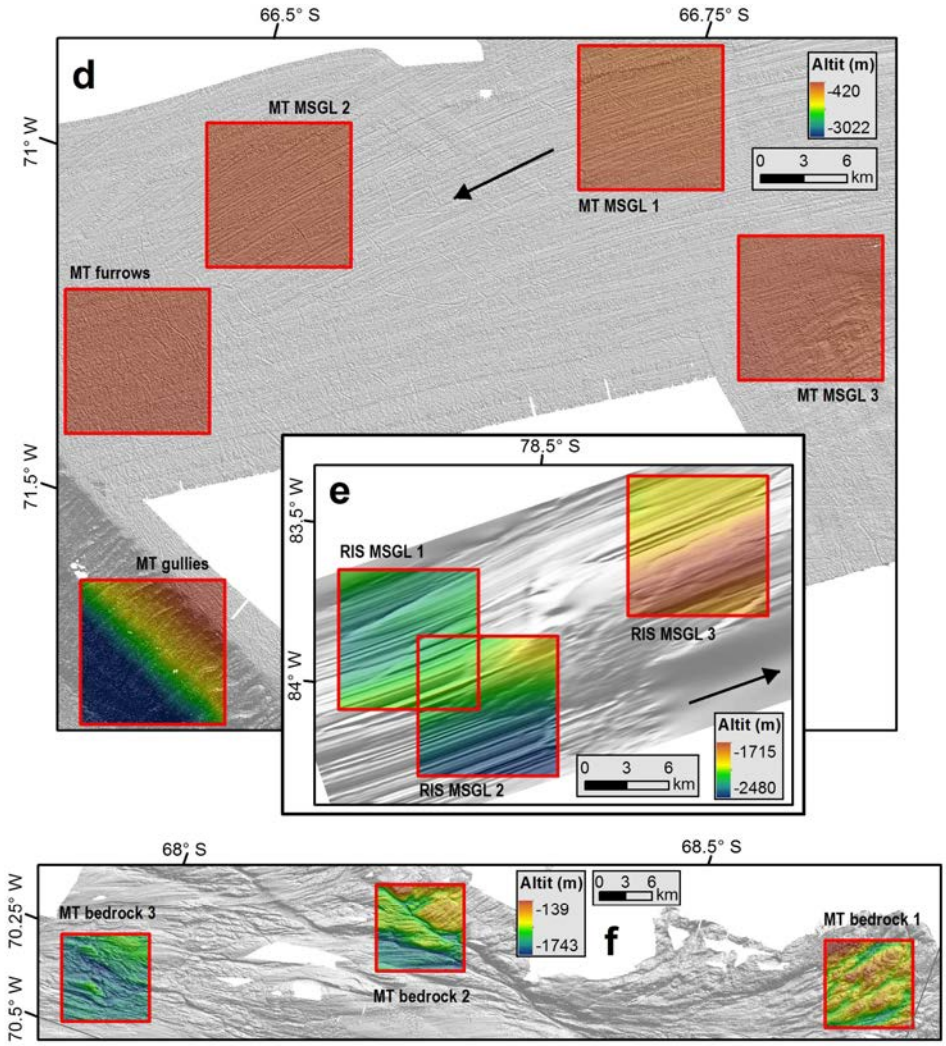

196

197

198 Figure 1. Locations of the datasets from various ice stream beds worldwide (see also Table 1). The samples for
199 which the Fourier analysis has been run are represented by red squares. (a) the marine Amundsen Sea
200 Embayment Dotson-Getz paleo ice stream bed (Antarctica), sampled in five different areas from upstream
201 streamlined bedrock to downstream MSGL; (b) the marine Pine Island paleo ice stream bed (Antarctica), with
202 two MSGL-dominated terrains and one iceberg-furrow dominated terrain; (c) the lower Athabasca Region
203 terrestrial paleo ice stream bed (Canada), with a sample of a flat fluvial open plain, a fluvially dissected plateau
204 and one of MSGLs partly modified by fluvial processes; (d) the marine "distal" Marguerite Trough paleo ice
205 stream bed (Antarctica), with samples of shelf break gullies, iceberg furrows and MSGL; (e) the extant Rutford
206 Ice Stream bed (Antarctica), where three MSGL samples have been analyzed; (f) the 'proximal' Marguerite
207 Trough paleo ice stream bed (Antarctica), with three samples of bedrock, with modest or absent streamlining.
208 Black arrows show ice-flow direction.

209

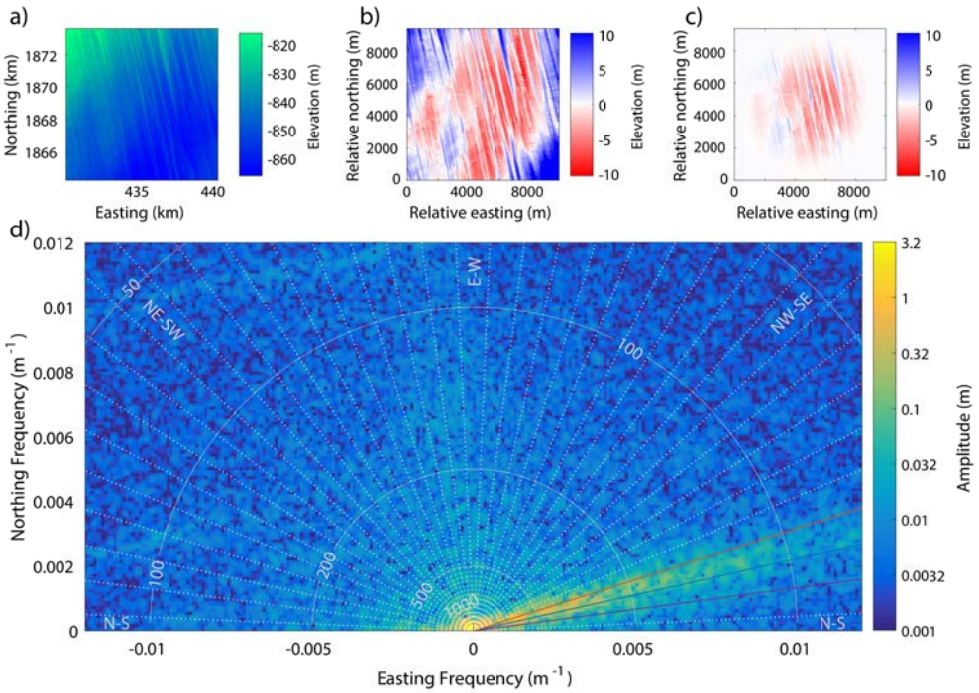

Figure 2. Example data and 2D Fourier spectrum from the Pine Island (Antarctica) dataset, PI_MSGL_1. a) Raw input data (elevation relative to the sea surface) sampled within a 10 x 10 km window. Raw depth observations have a resolution of 1 m. b) Detrended data. c) 2D Hann-windowed and detrended data. d) Frequency domain depiction of the data in (c). In (d) the background colors illustrate the average amplitude of topographic variations with specific easting and northing frequencies. Semi-circular lines of equal wavelength (labelled in m) contour the frequency space. Lines extending radially from the bottom-center at 5° increments represent features in the data with specific orientations. Cardinal and intermediate directions (e.g. NW-SE) for corrugation orientations are labelled. Most orientations are dotted white, whereas orientations with the largest amplitudes are colored for consistency with Fig. 3. For this case, our quantitative approach (Fig. 3) identifies that these MSGLs trend 12.6° W of N, with maximum normalized wavelength λ (i.e. lateral spacing) of 690 m.

2.3 Quantification of dominant wavelengths and orientations

We examined how topography varies for the full range of possible θ (i.e., orientations from -90° to 90°) by extracting 1-dimensional slices through the 2D spectra, equivalent to calculating a 1-dimensional topographic spectrum with specific orientations. Our 2D spectra (e.g. Fig. 2d) exhibit consistent 'speckle' across the entire frequency space. This speckle represents noise that can be reduced by averaging over both orientations and wavelengths. We extracted amplitude profiles logarithmically sampled in wavelength along every orientation at 0.2° intervals. We then calculated 5° running means across orientations and

231 smoothed the amplitudes across wavelengths with a LOESS filter implemented in Matlab.
232 We found that a smoothing span of 1/5 of a decade in λ (1/5 of an order of magnitude; e.g.
233 Fig. 3a) offered a qualitatively good balance between noise suppression and wavelength
234 resolution. The topographic amplitude as a function of wavelength for orientations spaced
235 every 5° is shown in Fig. 4a, centered on the orientation with peak amplitude.

236 Topography is naturally characterized by large amplitudes at long wavelengths and
237 smaller amplitudes at shorter wavelengths [*Sayles and Thomas, 1978*]. For each of our
238 DTMs, we identified the background relationship between wavelength (λ) and amplitude by
239 calculating the median amplitude as a function of λ across all orientations, θ. We refer to
240 these median amplitudes as the background spectra. Consistently oriented topographic
241 features that exhibit periodicity (i.e. a high degree of spatial regularity) have amplitudes that
242 rise above these median, background, topographic amplitudes. To specifically examine these
243 periodic features, we normalized the amplitudes for each θ by the background spectra (Fig.
244 3b). Because the normalized amplitudes are highly sensitive to the background spectra, the
245 median values that serve as the basis for normalization were smoothed with a span twice that
246 used for each θ in the non-normalized plots (e.g. Fig. 3a). This approach allows us to
247 rigorously and automatically identify the orientations and wavelengths of periodic, spatially
248 regular topography.

249 Strongly periodic features within the DTMs have large median-normalized amplitudes
250 (Fig. 3b). To emphasize those orientations with the greatest normalized amplitudes, we
251 identified all orientations with normalized amplitude reaching at least 50% of the largest
252 normalized amplitude among all orientations and attaining normalized amplitudes > 3 (these
253 threshold choices are arbitrary, and only for visualization). These orientations are colored
254 consistently in Figs. 2d and 3. All other orientations are dotted grey. Several examples
255 detailing the results of our approach with simple, synthetic data are included as Supporting
256 Information (Figs. S1-S6).

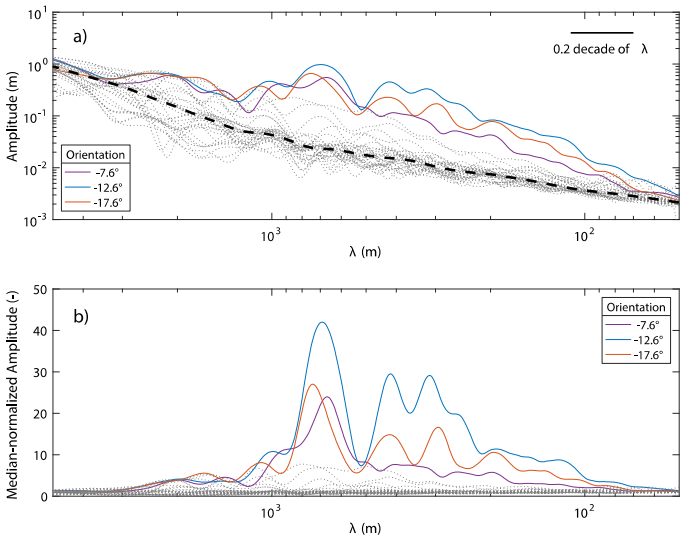

Figure 3. Topographic amplitude as a function of wavelength for orientations spaced every 5° for PI_MSGL_1. Each orientation is represented by a colored or grey dotted line. (a) Unnormalized amplitudes, with the median of all orientations shown by the black dashed line. Amplitudes are smoothed with a span of 1/5th decade of λ. (b) Amplitudes normalized by the median, demonstrating how much larger than the background spectra a certain feature (the MSGLs, in this case) is. For (a) and (b), as well as in Fig. 2, orientations with the largest normalized amplitudes are colored and labelled by their trends in the legend (orientations relative to North), whereas smaller normalized amplitudes are dotted grey. This representation shows that the MSGLs with a -12.6° W of N trend reach amplitudes up to 42 times higher than the median amplitude at a wavelength of 690 m.

2.4 Resolution of the analysis

Our ability to resolve the spectral characteristics of topography is constrained by the limitations of the input DTMs. As the input data are posted at (grid) horizontal resolutions ranging from 2 to 30 m (Table 1), the high-frequency limit beyond which we cannot identify unaliased topographic variations, the Nyquist frequency, varies from 0.25 to 0.017 m^{-1}, equivalent to λ = 4 to 60 m. At the other extreme, for long wavelengths, we approach a limit beyond which only one or a few λ fit within the extent of the 10 km DTMs. For this reason, we limit our discussion to those features with λ < 3 km; our interpretable range is therefore 60 m < λ < 3 km.

The vertical resolution of our multi-beam bathymetry and LiDAR datasets is, in some cases, as coarse as 3 m (Table 1). However, the spatial averaging implicit within the spectral analysis allows us to resolve periodic features with much greater precision. Therefore, we use empirical assessments to demonstrate the vertical resolution of our analyses. Many of the amplitudes for orientations not associated with MSGLs cluster tightly around each other and

281 the median amplitude, and follow consistent slopes in the spectral log-log plots for $\lambda < 500$ m
282 (e.g. Fig. 3a). Similar, consistent slopes are commonly reported for a wide range of surfaces
283 [*Brown and Scholtz, 1985; Sayles and Thomas, 1978*]. We interpret these consistent slopes as
284 indications that the spatially aggregated amplitudes of the DTMs are accurately characterized
285 even to scales < 0.01 m (less than the specified vertical resolution of an individual elevation
286 measurement).

287 The nature of the bed data collected from the extant Rutford Ice Stream limits our
288 ability to fully analyze their spectra, as above. These bed-elevation data were collected along
289 radio-echo sounding profiles at 7.5 m intervals across the crests of the MSGLs, allowing for
290 spectral analysis across crests of features with a wavelength as fine as 15 m. However, profile
291 spacing along the crests of the MSGLs was 500 m. Although we used a cubic interpolation to
292 resample these data to a 10 m grid, the original data resolution prevents us from
293 characterizing periodicity with wavelength $\lambda < 1$ km for orientations not directly aligned with
294 the MSGLs (normal to the radar profiles). In the absence of complete 180° orientation
295 sampling, we are unable to normalize the spectra and identify maxima in λ in the same
296 manner described above. Thus, the Rutford Ice Stream spectra are presented only in their un-
297 normalized forms (Fig. 5c).

298

299 # 3. RESULTS

300 ## 3.1 MSGL periodic wavelengths and orientations

301 The discrimination of MSGLs is enabled by comparison of topographic amplitudes in
302 one direction with those of all other directions (Fig. 3b). In the case of PI_MSGL_1, the most
303 obvious MSGLs have a crest to crest spacing of 700 m and trend slightly west of due North
304 (Fig. 1b). Our spectral analysis bears this out, indicating that the dominant wavelength is 690
305 m and is oriented 12.6° W of N (Fig. 3b). However, our method also reveals subtlety in the
306 DTM which is not immediately apparent. Overprinting the MSGLs with 690 m spacing, we
307 also find strong periodicity at 310 and 420 m wavelengths. The peaks and troughs in these
308 normalized wavelengths are well-defined, with obvious separation amongst the multiple
309 peaks. A similar pattern of peaks and troughs in the normalized spectra is also found in
310 adjacent orientations, with above-average amplitudes bracketing the dominant MSGL
311 orientation by ±5°.

In a different MSGL setting (MT_MSGL_2), our analysis identifies a dominant wavelength of 310 m oriented at 131.4° E of N (Fig. 4a). More subtle peaks in the spectra are found at longer and shorter wavelengths. In contrast, the LAR_fluvial dataset, a terrestrial landscape with no MSGLs but abundant fluvial erosion features, has no clear maxima or minima in periodic orientation or wavelength. Despite several-hundred-meter characteristic widths for the channels apparent in the DTM (Fig. 1c), these features are not periodic and all median-normalized amplitudes are less than 3 (Fig. 4b).

When we examine the full set of MSGLs, we find that multiple wavelength peaks within a single topographic dataset are common. These peaks in MSGL amplitude reach up to 42 times higher than the median amplitudes from all orientations (background amplitudes) (Table 1 and Fig. 3) and are generally sharp, with widths at half-height on the order of the width of our low-pass filter (Fig. 4c). Clear gaps in the normalized amplitudes exist between the peaks. Neither the peaks nor the gaps in amplitude are found at the same wavelengths among the different MSGL settings (Fig. 4c, S7). The dominant wavelengths, those with the maximum normalized amplitudes, are found between 320 m and 1200 m, apart from the terrestrial LAR_MSGL which is discussed in section 3.4. While the dominant wavelengths span a relatively narrow range, amplitudes reaching several times the background amplitude occur in many settings for $\lambda > 2000$ m and for $\lambda < 100$ m (Fig. 2, 3b, 4a, 4c, S7). The latter is towards the resolvable limit of short wavelength topography. However, these broad- and fine-scale corrugations have significantly weaker amplitudes than those at wavelengths between approximately 320 and 1200 m. Topographies without clear MSGLs, and even landscapes dominated by streamlined bedrock and crag-and-tail features, do not have dominant wavelengths characterized by normalized amplitudes as high as those from the MSGL landscapes (nowhere do they exceed 8), and have amplitude peaks that often span a wider range of wavelengths than the MSGLs (Fig. 4d and Table 1).

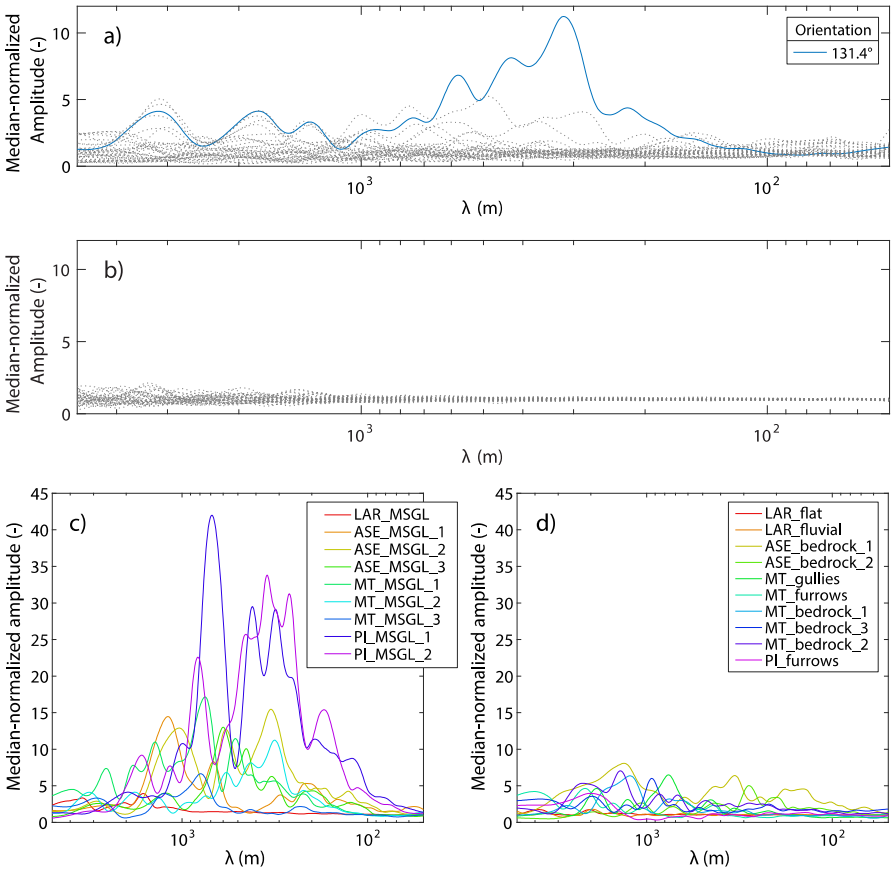

Figure 4: Comparison between MSGL-rich and other types of terrain. (a) the spectral signature of the Marguerite Trough paleo ice stream bed, rich in MSGL (MT_MSGL_2) compared to (b) a fluvially-incised landscape (LAR_fluvial), with no MSGLs. (c) Normalized amplitudes for the dominant orientation of all analyzed MSGL samples compared to (d) that for all sampled non-MSGL terrains. The Rutford Ice Stream data are not plotted in (c) as noted in the text.

3.2 Amplitudes of MSGLs and other topographies

Normalization of each orientation's spectrum by the background spectra renders the most periodic features, such as MSGLs, immediately apparent. However, normalization presents the amplitudes of periodic wavelengths only in a relative sense, obscuring the true height of MSGLs. Within the detrended data for PI_MSGL_1 (Fig. 2b), trough-to-crest heights of some individual MSGLs exceed 10 m. This trough-to-crest measurement is twice the height of our 'amplitudes', which are defined in the sense common to physics and signal processing as one half the trough-to-crest range. However, the amplitudes of many MSGLs in

PI_MSGL_1 are clearly lower. For example, the average amplitude of the dominant λ = 690 m MSGLs, as calculated by our Fourier analysis, is 1.0 m (Fig. 3a). This amplitude is 42 times greater than the median, background amplitude of 0.023 m at the same wavelength (Fig. 3a and 3b).

Examination of the un-normalized spectra for each MSGL dataset reveals that, within their characteristic 300 – 1200 m wavelengths, MSGL amplitudes show a tendency to increase with wavelength and average about 0.2 m at λ = 300 m and 1.0 m at λ = 1200 m (Fig. 5c). Thus, at the long end of the wavelength spectrum, these MSGL amplitudes are consistent with the 1 – 3 m average trough-to-crest ranges reported previously [*Spagnolo et al., 2014*].

The amplitude spectra of MSGLs share similar features to those of other landforms and produce a power-law spectral signature, with $A = a\ \lambda^b$, where A is amplitude, and a and b are parameters fit to the data [*Sayles and Thomas, 1978; Huang and Turcotte, 1990*]. Our use here of true topographic amplitudes (Fourier coefficients), rather than power, differs slightly from convention, where power law spectra are shown through power spectral densities. Power in power spectral densities is related to the square of amplitude, and thus the b values in our amplitude spectra are half as large as those in power spectra [cf., *Perron et al., 2008*]. The non-MSGL terrains analyzed here follow this general pattern of increasing amplitude with increasing wavelength, with b varying slightly amongst topographies between 1.5 and 2.3 (Fig. 5a). The spectra of MSGL topographies, along their dominant orientations (Fig. 5c), are generally bracketed within a similar range of $A(\lambda)$, from a few decimeters to a few meters, as apparent from their lying between the same black, power law lines drawn in all plots of Figure 5. However, the median spectra of MSGL background topographies (i.e., topography not oriented with the MSGLs themselves) are strikingly different from both the non-MSGL topographies and the dominant MSGL orientations. These background MSGL spectra have amplitudes depressed by a factor of 10 or more (at λ = 500 m) and slopes also depressed over a broad range of λ, from 100 m (below the typical λ of MSGLs) up to about 1300 m (greater than the maximum dominant λ of MSGLs) (Fig. 5b). Thus, where MSGLs are present, the vertical relief of landscape features not oriented with MSGLs is considerably subdued relative to landscapes without MSGLs.

These results apply to all analyzed MSGL settings, including the extant Rutford Ice Stream bed. The exceptions to these general patterns are the three LAR datasets, from the

terrestrial landscape of northern Alberta, and the iceberg furrows from the Antarctic marine settings (both PI_furrows and MT_furrows). The LAR landscapes have considerably smaller amplitudes than the other topographies (smaller *a* values), but with similar spectral slopes (*b* values of about 2). The two furrowed topographies have lower spectral slopes (*b* values of about 0.5), similar to the background spectra of MSGL datasets. These two exceptions are discussed in section 3.4 and 4.2.2, respectively.

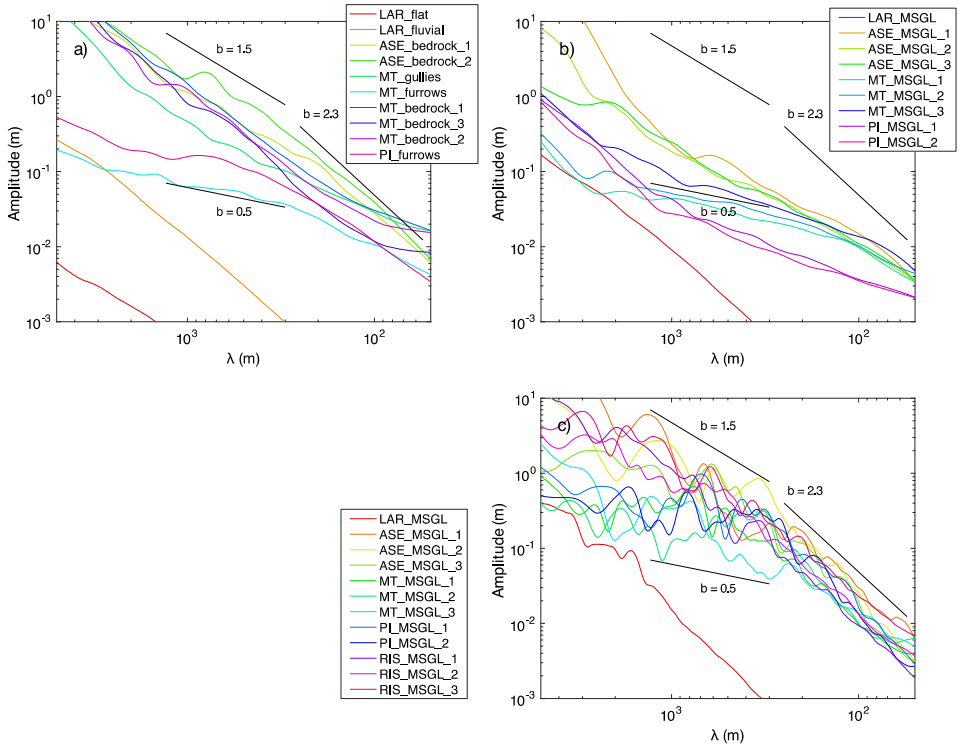

Figure 5: a) Median spectra of non-MSGL topographies. b) Median spectra of MSGL topographies. c) Spectra of MSGL topographies in the dominant orientation. Normalized spectra, for example in Fig. 5, result from the division of the amplitude at the dominant orientation by the median amplitude of all spectra. Lines illustrating specific spectral slopes are shown in black and identified by the exponent in $A = a\ \lambda^b$. In each panel, the parameter sets for each of the three lines are identical.

3.3 Downstream variations in amplitude and wavelength along the bed of a former ice stream

The extent of the bathymetry from the Getz paleo ice stream bed (Amundsen Sea Embayment, Antarctica, Fig. 1a) allows us to identify how topographic spectral properties vary along over 50 km of former ice stream bed. This setting presents a morphological configuration that is typical of many Antarctic paleo ice stream beds, with upstream bedrock outcrops progressively transitioning downstream into crag-and-tail and MSGL features [*Wellner et al., 2001*]. The results of our approach show that the streamlined bedrock and/or crag-and-tail topography of the upstream portions (ASE_bedrock_1 and 2) consist of above-average median-normalized amplitudes, at many different orientations and wavelengths (Figs. 6d-e). Specifically, the number of orientations with above-average median-normalized amplitudes spans up to 45°, a much greater value than the typical 20° for MSGL landscapes, while normalized amplitudes (up to 8) are much lower than those of the MSGLs (Fig. 4c). The dataset furthest upstream (ASE_bedrock_1), largely composed of streamlined bedrock with a few MSGLs within a region to the NE, has highest normalized amplitudes at wavelengths between 1,000 and 2,000 m, as well as 200 – 500 m (Fig. 6e). Downstream, the topography is dominated by crag-and-tail features (ASE_bedrock_2) and characterized by high-normalized amplitudes across a wide range of wavelengths from 100-1000 m (Fig. 6d). The middle dataset in the sequence (ASE_MSGL_1) is mostly characterized by MSGLs, with dominant wavelengths of ~800 and ~1200 m, and amplitudes up to 15 times greater than the median amplitude (Fig. 6c). Very large median-normalized amplitudes are also present in the MSGL datasets further downstream, but at clearly different wavelengths. In ASE_MSGL_2, we find peak amplitudes at ~350, ~600 and ~1000 m wavelengths, while in ASE_MSGL_3, the furthest downstream dataset, only wavelengths between 450 and 600 m have the highest amplitudes (Fig. 6a-b). Overall, a striking difference is found between the Fourier signatures of subglacially-modified bedrock-cored landforms and MSGLs, with a clear tendency towards more strongly peaked wavelengths in the MSGLs downstream. Within the MSGL datasets, we find no consistent wavelengths even among datasets spaced just 10 km apart

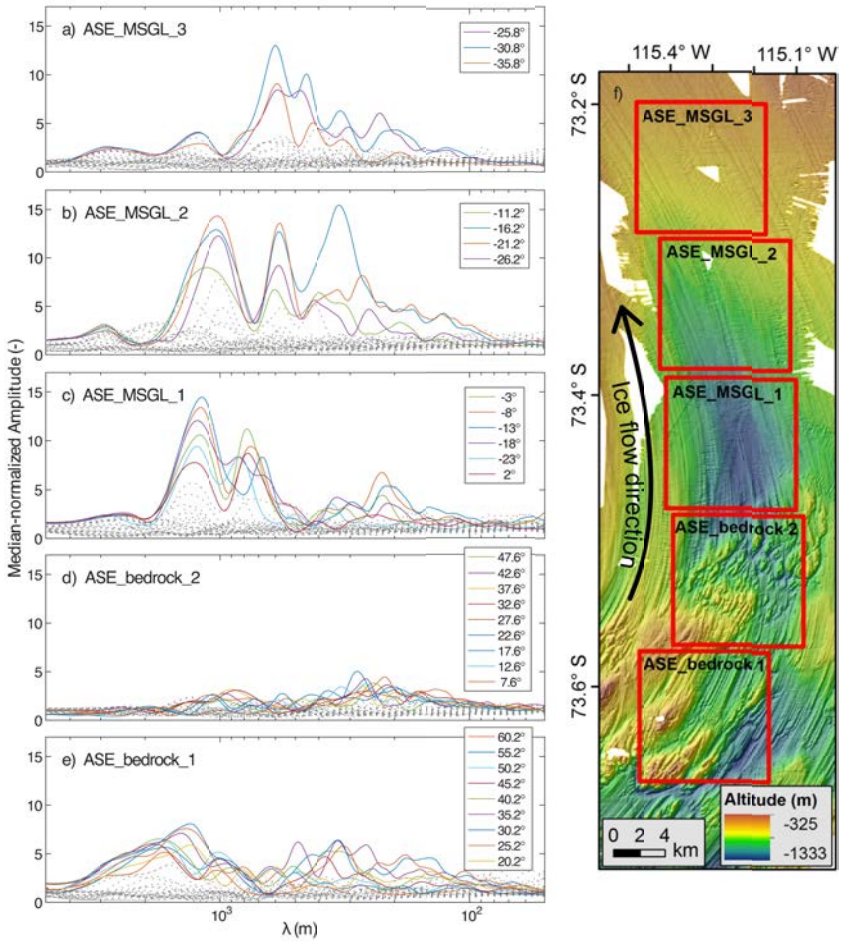

Figure 6. Datasets for the Getz paleo ice stream bed (Amundsen Sea Embayment), progressing downstream (bottom to top) from streamlined bedrock in the south, to crag-and-tail features, then MSGLs to the north. Normalized spectra from the 5 red squares (f) are shown in panels (a) – (e).

To evaluate the extent to which these dominant wavelengths vary along-flow, we resampled the ASE topography (Fig. 6f) with 75% overlap between 10 km samples, spaced evenly every 2.5 km. These resampled data are identified as ASE_MSGL_0.25, _0.50, etc., from the transition out of the bedrock-dominated topography, down to ASE_MSGL_3. The orientations with the peak-normalized amplitudes are shown in Fig. 7a. We find that, with this greater spatial resolution, individual dominant wavelengths correlate up and downstream, and trends among these peak wavelengths are identifiable. We identify four trends in peak wavelength that appear to lengthen over 5, 8, 6, and 4 successive samples (red lines in Fig.

7a). We also find weaker evidence of shortening or steady wavelengths (blue lines in Fig. 7a). To identify the magnitude of these trends, we measure the wavelength of each local amplitude maximum and fit linear models to the base 10 logarithm of the wavelengths, as a function of position along the paleo ice stream. The slopes of these lines, bounded with 95% confidence intervals and identified from large to small wavelengths, reveals that these MSGL wavelengths increase at the rates of $2.3^{+1.8}_{-1.7}$% km^{-1}, 0.95±0.52% km^{-1}, 2.7±1.0% km^{-1}, and $2.7^{+3.4}_{-3.3}$% km^{-1} respectively. Linear regression of wavelength on position yielded more widely varying estimates of the growth rate. To identify the most robust average relationship amongst the four trend lines, we employ a generalized linear mixed effect model, fit with a random effect of trend line. This modeling framework allows us to estimate a shared, average rate of downstream wavelength change, while allowing for different initial wavelengths. The shared average rate of wavelength increase is 1.7±0.52% km^{-1}. We also identify two trends, spanning shorter portions of the MSGL field, that reveal steady wavelengths, or wavelengths that decrease downstream. The steady wavelengths are found among those DTMs closest to the bedrock at λ = 1200 m, similar to the wavelengths of sculpted bedrock features. Towards the downstream end of the analyzed section of seafloor, we also identify a set of peak wavelengths that appear to decrease from 1500 to 1200 m over 5 km (three DTMs).

Among this set of resampled DTMs, we find that the un-normalized amplitudes (Figure 7b) differ between those DTMs containing the largest proportion of bedrock, and those DTMs dominated by MSGLs. ASE_bedrock_2, ASE_MSGL_0.25, and ASE_MSGL_0.50 reach amplitudes approximately half an order of magnitude greater than the MSGL DTMs. Among the MSGL DTMs, no along-flow variation in amplitude for $\lambda <$ 600 m is found, while for $\lambda >$ 600 m there is a tendency towards reduced amplitudes downstream.

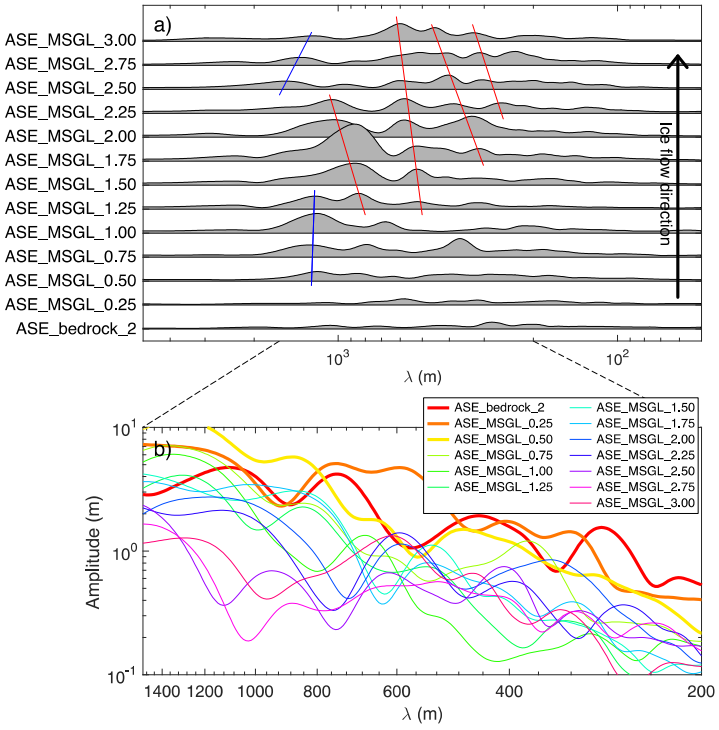

Figure 7: Along-flow variation in wavelength and amplitude from the Getz paleo ice stream bed (Fig. 6). (a) Normalized spectra for the resampled, 75% overlapping topographic datasets with paleo ice flow progressing from bottom to top. Only the orientation with the largest normalized amplitude is shown for each DTM, and normalized amplitudes are shown at scale relative to each other. The largest normalized amplitude, at ASE_MSGL_1.75, reaches 27 times the amplitude of its background spectra. Four increasing trends in wavelength are identified by red lines and are discussed in the text; one steady and one decreasing trend are marked in blue. (b) Un-normalized amplitudes for the same DTMs and orientations shown in (a), spanning the range of wavelengths most commonly containing MSGLs. Spectra from those DTMs containing the largest proportion of bedrock (ASE_bedrock_2 – ASE_MSGL_0.50) are shown with a heavier line weight.

3.4 Present-day active and paleo terrestrial MSGLs

The un-normalized spectra of the Rutford Ice Stream are qualitatively similar to the spectra of the paleo ice streams (Fig. 5c). In terms of their amplitudes and their spectral slopes, these extant features are indistinguishable from MSGLs formed by the paleo Pine Island, Marguerite Trough and Getz ice streams.

Most of the analyzed paleo ice stream beds belong to marine settings and are thus well preserved (Tab. 1). However, the Lower Athabasca dataset is characterized by a terrestrial paleo ice stream bed. The LAR_MSGL dataset consists of a MSGL field modified by terrestrial processes, and exhibits a subdued Fourier spectral signature when compared with

offshore counterparts. The peak amplitude for LAR_MSGL is only 3.9 times greater than background, lower than the typical normalized amplitudes of 10 or higher. It also occurs at an especially large wavelength (1600 m) (Figs. 4). This is possibly due to poor preservation related to fluvial and hillslope erosion and deposition following MSGL formation. Alternatively, the LAR MSGLs may have formed under different boundary conditions than in the marine settings or had insufficient time to develop.

4. DISCUSSION

4.1 The distinctive, Fourier spectral signature of MSGLs

The 2D Fourier analysis has quantitatively demonstrated that MSGLs are characterized by:

(i) several dominant wavelengths whose spectral amplitude rises sharply above the background amplitude spectra, bounded by wavelength gaps with very low amplitudes,
(ii) amplitudes of decimeters to a few meters,
(iii) median-normalized amplitudes of MSGLs are usually an order of magnitude larger than the amplitudes in all other orientations, and up to 5 times larger than other, non-MSGL topographies,
(iv) a narrow range of dominant orientations (< 20° complete range),
(v) a limited interval of wavelengths with greatest amplitudes (~ 300-1200 m)

Some of these results are consistent with estimates from previous qualitative and quantitative studies. For example, MSGL heights of a few meters have been reported before [*Spagnolo et al., 2014*], although here we have revealed periodic features with average amplitudes of down to the scale of decimeters. The reported spacing between adjacent MSGLs from various settings [e.g. *Ottesen et al., 2005*] also generally fit within the 300-1200 m interval highlighted here. A previous study of glacial lineations across terrestrial Canadian Arctic sites, where 1D Fourier analysis was applied to transects drawn across satellite images, also revealed comparable wavelength ranges (150-750 m) [*Fowahuh & Clark, 1995*]. However, this study is the first time a completely automated 2D Fourier analysis is applied, and to a wide variety of MSGL settings. Numerical ice stream models that consider bed topography could adopt (i)-(v) as input data; numerical models attempting to evolve a sedimentary bed into landforms can use these results as tests for their outputs.

Characteristics (i)-(v) are found among all analyzed MSGL datasets and are distinct from those identified for other landforms analyzed in this study. Such a distinct signature offers some promise for the development of tools for the automated identification of MSGLs and the extraction of metrics without the need to map individual features. This is a significant advance, as mapping MSGLs has proved to be difficult, given the spatial continuity of these highly-elongated corrugations and the care necessary to judge what constitutes a mappable feature [*Spagnolo et al., 2014; Piasecka et al., 2016*]. The automated identification of MSGLs based on their spectral signature in the frequency domain could also be extremely useful in the study of buried ice stream beds, such as those imaged from 3D seismic data across glaciated continental margins [e.g. *Dowdeswell et al., 2006; Graham et al., 2007; Andreassen et al., 2009; Piasecka et al., 2016*].

4.2 MSGLs as a patterned phenomenon and implications for formational theories

The occurrence of a small number of dominant wavelengths within a narrow range of orientations demonstrates, quantitatively, that MSGLs represent a patterned, periodic topography, with regularly spaced landforms of similar shape and size. These characteristics are typical of spatially self-organized landscapes [*Hallet, 1990*].

A number of hypotheses have been proposed for MSGL formation. Proponents of subglacial mega-floods suggest that MSGLs are formed by erosional vortices within turbulent sheet-floods capable of decoupling the ice sheet from its bed [*Shaw et al., 2008*]. The rilling instability hypothesis proposes that MSGLs are erosional landforms that emerge at the ice-water-bed interfaces from positive feedbacks in the unstable, coupled flow of ice, water and sediment [*Fowler, 2010*]. MSGLs could also be the product of sediment deformation [*Boulton, 1987; Clark et al., 1993*]. Specifically, the pressure-gradient hypothesis suggests that MSGLs are formed through gradients in ice pressure over deforming sediment, with MSGLs emerging from an uneven bed as a result of stoss-side erosion and lee-side deposition into cavities [*Barchyn et al., 2016*]. Finally, the groove-ploughing hypothesis invokes erosion via basal ice keels ploughing through soft sediment [*Tulaczyk et al., 2001; Clark et al., 2003*]. Although sedimentological evidence from MSGLs exposed on land in Arctic Canada suggests that some lineations have an (at least partially) erosional origin [*Ó Cofaigh et al., 2013*], other studies have shown that MSGLs are constructed by the continuous accretion of sediment [*Spagnolo et al., 2016*]. From our analysis, it is not possible to determine whether

547 the MSGLs presented here are erosional, depositional or a combination of both. However, our
548 data lead to five considerations (detailed below), which are relevant to our understanding of
549 subglacial processes and the formation of MSGLs.

550 **4.2.1 Comparison between MSGLs and bedrock-related glacial landforms**

551 The 2D Fourier spectral analysis has revealed that the erosion of streamlined bedrock
552 by flowing ice does not produce the regular topographic signature that we see where MSGLs
553 are present. Similarly, deposition in the lee of bedrock knobs, producing crag-and-tail
554 features, fails to generate 2D Fourier spectra similar to that of MSGLs. This is certainly the
555 case for the Getz paleo ice stream bed, where MSGLs and bedrock-related features are only a
556 few kilometers apart and yet have distinct spectra (Fig. 6c-d). Deposition or erosion along an
557 ice stream bed, when anchored to bedrock outcrops, does not generate the regularly spaced
558 topography of MSGLs. For MSGLs to generate periodic topography, sediment must be able
559 to move freely without fixed anchor points.

560 The streamlined bedrock and crag-and-tail datasets show some above average median
561 amplitude values (colored lines in Figure 6d). However, these values are found across a wide
562 range of orientations (up to 45°) and wavelengths (spanning an order of magnitude or more).
563 Both these orientation and wavelength ranges far exceed those of MSGLs (Fig. 6). Bedrock-
564 related topographies could reflect wavelengths and orientations not wholly dependent on the
565 erosive action of ice flow. For example, they could represent the geomorphological
566 expression of structures in the sedimentary bedrock or rock fracture patterns [*Krabbendam*
567 *and Bradwell, 2011*]. However, the spread of large amplitude orientations for bedrock-
568 dominated terrains, roughly aligned with the overall S-N ice-flow direction, is likely to reflect
569 the tortuosity of basal ice flow in the face of large-scale bedrock obstacles. These basal flow
570 directions have the potential to offer a new constraint on the plasticity of basal ice.

571 Spectral analysis is also capable of resolving the signature of multiple bedforms
572 within a single DTM. Within ASE_bedrock_1 (Fig 6e), we find features with normalized
573 amplitudes near 5 spanning a wide range of wavelengths from 800-3000 m, reflecting the
574 eroded bedrock. We also identify enhanced amplitudes over a 200-500 m wavelength range
575 with a narrower range of orientations (20°, rather than the 50° range of orientations present at
576 800-3000 m), which are consistent with the spectral signature of MSGLs. These MSGLs are
577 apparent in the NE portion of ASE_bedrock_1 (Fig 6f). This demonstrates that Fourier

analysis can identify and distinguish two different landforms within the same setting, as well as their orientation ranges and roughness.

4.2.2 Downstream variability of MSGL wavelengths and amplitudes

The groove-ploughing hypothesis suggests that MSGLs may be formed by the ploughing action of basal ice keels through soft sediment [*Tulaczyk et al., 2001; Clark et al., 2003*]. The keels are hypothesized to form either by convergent flow or from differential ice molding when the basal ice flows over outcropping bedrock. In this latter case, one would expect MSGLs found downstream of outcropping bedrock to have wavelengths comparable to those of the bedrock upstream [*Clark et al., 2003*]. The groove-ploughing hypothesis also suggests that keels should progressively melt downstream because of frictional heating, thus broadening the MSGLs and reducing their amplitude, while their wavelength should remain constant [*Clark et al., 2003*]. These aspects were tested along the Getz paleo ice stream bed. Contrary to groove-ploughing prediction, the large number of significant wavelengths, associated with modest (lower than 8 times the median) amplitudes of the streamlined bedrock and crag-and-tail features, do not match the few dominant wavelengths typical of the MSGLs located immediately downstream (Fig. 6-7).

Rather than preserving the spacing imprint of upstream bedrock, we find that most of the multiple, distinct MSGL wavelength peaks within a DTM evolve towards longer wavelengths downstream. Over the approximately 20 km between ASE_MSGL_1 and ASE_MSGL_3, a given peak wavelength increases by an average of 40%. New peak wavelengths emerge at intervals downstream (at wavelengths between 200 and 300 m, the lower end of the MSGL range), and increase until they reach their maximum cutoff, near 1200 m (Fig. 7). At the base of ice streams, both sediment and ice will move down-flow over time. Thus, through the assumption that downstream bedforms reflect temporal evolution, we conclude that individual MSGL spectra evolve continuously, even under conceivably steady conditions, just as a steady, turbulent, jet continuously casts off eddies that grow in scale prior to dissipating in a surrounding viscous fluid.

Two potential exceptions to the trend of downstream-increasing wavelength exist. One is found close to the upstream end of the MSGL field, near the outcropping bedrock, where a similar, peak wavelength near 1200 m is identified across four consecutive datasets. A similar dominant wavelength is found in the bedrock-rich dataset further upstream (ASE_bedrock_1) (Fig. 6). Thus, this exception might represent the only evidence of bedrock-related groove-ploughing in our study. The other is toward the downstream end of

611 the MSGL field, where wavelengths decrease over 5 km (across three consecutive datasets).
612 This short-distance trend is found at the upper limit of the wavelength range of MSGLs and
613 might be related to non-MSGL topography.
614 The amplitudes reveal different patterns for different wavelengths. Decreased
615 downstream amplitudes, observed for wavelengths >600 m, are in agreement with predictions
616 of the groove-ploughing theory. However, we find no consistent change in MSGL amplitudes
617 for wavelengths <600 m. Overall, while more MSGL settings should be analyzed to reach
618 broader conclusions, most of the results presented here appear inconsistent with the groove-
619 ploughing theory, at least in its present form. Instead, these results provide support for
620 theories that invoke the growth of dominant wavelengths via positive feedbacks occurring at
621 an unstable ice-bed interface.
622
623 **4.2.3 Instability as a potential ingredient in the formation of MSGL**
624 Instability theories predict that there is a wavelength that grows most rapidly and
625 tends to naturally dominate over others, with the system evolving towards a periodic
626 landscape [e.g. *Baas, 2002*]. Such models have been developed for a variety of glacial
627 bedforms, including flutes [*Schoof, 2007*], drumlins [*Hindmarsh, 1999*] and MSGLs [*Fowler,*
628 *2010; Fowler and Chapwanya, 2014*]. The distinct MSGL spectral signature, multiple high-
629 amplitude wavelengths within the MSGL fields, and the downstream coarsening of MSGL
630 wavelengths, are consistent with hypotheses that see instability-driven positive feedbacks
631 playing a key role in the formation and evolution of these sedimentary subglacial bedforms.
632 However, no current theories predict multiple peak wavelengths within a single patch of ice
633 stream bed. We suggest that the downstream increase in wavelength and the observation of
634 multiple peak wavelengths are consistent with a continuously evolving pattern of bedforms.
635 Thus, the spectral characteristics of an ice stream bed may not be strictly deterministic, even
636 under steady conditions. An observed MSGL pattern could be created by many different ice
637 stream characteristics. This challenges the assertion that MSGL characteristics may at some
638 point be inverted for paleo ice-flow characteristics [*Barchyn et al., 2016*]. MSGL evolution
639 may be affected by pattern coarsening, a phenomenon already suggested for the formation of
640 dunes [e.g. *Fourrière et al., 2010*]. Instabilities emerging at small wavelengths may
641 progressively grow in scale, increasing their wavelengths until the large wavelength limit (~
642 1200 m), at which point they dissipate under the influence of other basal processes. In this

643 view, the presence of multiple dominant MSGL wavelengths (Fig. 6) could indicate that new
644 MSGLs with short wavelengths are continuously formed while others dissipate.

645 **4.2.4 Relative amplitudes of MSGLs and their background topography**

646 Results show that MSGLs are characterized by modest amplitudes, from a few
647 decimeters to a few meters (Fig. 5c). Amplitudes of non-MSGL topographies are slightly
648 higher, but mostly within the same order of magnitude (Fig. 5a). However, MSGL spectra are
649 unique within our study due to the large difference between their amplitudes at dominant
650 orientation and those at other orientations. This difference has the potential to arise through
651 either the addition or subtraction of roughness (or a combination of the two) within the range
652 of MSGL wavelengths. In the roughness addition hypothesis, MSGLs are visually apparent
653 (Figs. 1 and 2) because they have been constructed by erosion and/or deposition on an
654 initially smooth topography. In the roughness subtraction hypothesis, MSGLs are visually
655 apparent because, on an initially rough topography, roughness at all but a narrow range of
656 orientations is removed.

657 The different non-normalized spectra can be interpreted through either lens. More
658 analyses of current ice stream beds are required to determine whether MSGLs emerge
659 through the addition or subtraction of roughness, or through both processes. Regardless, the
660 difference in ice stream bed amplitudes between ice-flow parallel and background (i.e. other)
661 orientations (Fig. 4c), along with the low spectral slopes (Fig. 5b), quantitatively demonstrate
662 that ice stream beds rich in MSGLs are characterized by reduced roughness, when compared
663 to other topographies. MSGL terrains are so smooth that, even when the MSGLs are
664 completely obliterated by the destructive action of iceberg keels (as in the two furrowed
665 datasets), the original signature of low background roughness remains largely unaltered (Fig.
666 5a). If MSGLs are an 'inevitable' emergent feature of coupled ice-(water?)-till flow, then
667 their relatively low-roughness configuration might represent the balance between MSGLs
668 tendency to grow and the ice stream's tendency to reduce basal drag. This study quantifies
669 amplitudes along and across the ice-flow direction for dominant wavelengths. As such, it
670 provides a better understanding of form drag imposed by subglacial landforms and might be
671 of relevance to inversions of ice-flow speed for basal properties [*Joughin et al., 2004;*
672 *Arthern et al., 2015*].

673 **4.2.5 MSGLs differ from typical fractal topographies**

674 Topography is often described as a fractal phenomenon, in that the morphology of
675 landforms maintains its scale invariant proportions [*Mandelbrot, 1982*]. This property is
676 present in some of the non-MSGL landscapes that we analyzed, which show amplitudes
677 increasing as a power-law function of wavelength (Fig. 5a). The exponents that best fit these
678 non-MSGL amplitudes ($1.5 < b < 2.3$) overlap the range appropriate for fractal surfaces ($1 <$
679 $b < 2$). The consistency of the scaling relationship over the nearly two orders of magnitude is
680 also in line with the concept of fractals [*Perron et al., 2008*].

681 In contrast, deviation from this simple fractal scaling is found in all the analyzed
682 MSGL datasets (Fig. 5b), similarly to the modification of amplitude spectra by periodic
683 stream valleys [*Perron et al., 2008*]. In our MSGL datasets, the consistent power-law
684 relationship of the background topography is clearly interrupted within the specific
685 wavelength interval of the MSGLs (300-1200 m), where amplitudes grow relatively slowly
686 with wavelength (Fig. 5b). The pace at which MSGL spectral signals grow (i.e. the slope of
687 the lines (b) in Figure 5b) is ~ 0.5, significantly lower than the values of 1.5 – 2.3 found
688 outside the MSGL wavelength interval and in all other non-MSGL settings we examined
689 (Fig. 6a, c). MSGL topography spectra also reveal a kink near 300 m, with lower b values for
690 $\lambda > 300$ m and greater b values for $\lambda < 300$ m. These properties are inconsistent with those of
691 fractals [*Huang and Turcotte, 1990; Perron et al., 2008*].

692

693 # CONCLUSIONS

694 We have applied 2D Fourier spectral analysis to 22 different topographies, mostly
695 associated with ice streams. These datasets include areas rich in MSGLs and, in some cases,
696 their bedrock-dominated areas upstream. Our technique allows for the objective
697 quantification of landscape metrics without the need for landforms to be subjectively or
698 individually mapped. Key conclusions are:

699 - MSGL fields consist of long corrugations with decimeter to meter amplitudes
700 periodically spaced every 300 – 1200 m. The periodic topography of MSGLs consists
701 of the superposition of multiple, similarly-oriented corrugations with distinct
702 wavelengths. MSGL patterns are spatially coherent, with regularly spaced landforms
703 of similar shape and size and produce a very distinct spectral signature that is not
704 found in the other landforms analyzed in our study. For such a periodic topography to

evolve, the anchoring effect of unevenly distributed bedrock knolls must play a minimal role in the formation of MSGLs.

- A formation hypothesis involving positive feedbacks occurring in an unstable subglacial system (instability theory) is supported by the observation of distinct, periodic MSGL wavelengths. Furthermore, along the Getz paleo ice stream bed in Antarctica, we find a) a downstream increase in wavelength, b) the appearance of new, short-wavelength MSGLs downstream, and c) a lack of relationship between wavelengths of MSGL spectra and the spectra of upstream bedrock. Together, these properties are compatible with an instability-driven formation of MSGLs, and challenge theories that require the ploughing of ice keels downstream of bedrock outcrops.
- MSGL spectral amplitudes are comparable to the amplitudes of topographies without MSGLs. However, the presence of MSGLs is coincident with an order-of-magnitude lowering of topographic amplitudes in directions not oriented with MSGLs. This indicates that the roughness of MSGL topographies is lower than that of any other terrains we analyzed.

The distinct signature of MSGL topographies is useful to develop tools for their automated identification. Our quantitative results may serve as a test for ice-water-bed interaction models or as input parameters for other numerical models seeking to understand the effect of topography on ice flow or attempting to evolve a sedimentary bed into landforms.

ACKNOWLEDGEMENTS

The research was funded by the NE/J004766/1 UK NERC New Investigator and a SAGES PECRE grants awarded to MS. The Amundsen Sea Embayment multi-beam data were acquired on cruise JR141 of the RRS James Clark Ross in 2006 (PI: R. Larter, British Antarctic Survey). The Pine Island multi-beam data were acquired on cruise OSO0910 (Chief scientists: J. Anderson, Rice University, and M. Jakobsson, Stockholm University). The Marguerite Trough multi-beam data were acquired on cruises JR59, JR71, JR157 and NBP0201. This research would not have been possible without the hard work of scientists and crew during these research cruises. John Anderson and Martin Jakobsson are thanked for providing easy access to the Pine Island bathymetries. We would like to thank John Shaw, Roger Hooke, an anonymous reviewer and the Editor, Bryn Hubbard, for their constructive comments and suggestions that have greatly improved the original manuscript. Underlying bathymetric/topographic data are available by request to the PI/chief scientists of the respective cruises/LIDAR acquisition programs. The spectral results can be accessed by

request to T. C. Bartholomaus (tbartholomaus@uidaho.edu) or M. Spagnolo (m.spagnolo@abdn.ac.uk).

REFERENCES

Anderson, J., M. Jakobsson, OSO0910 Scientific Party, 2010. Oden Southern Ocean 0910: Cruise Report, In: Meddelanden från Stockholms universitets institution för gelogiska vetenskaper. No 341, pp. 134

Anderson, J.B., S.S. Shipp, A.L. Lowe, J.S. Wellner, and A.B. Mosola (2002), The Antarctic Ice Sheet during the Last Glacial Maximum and its subsequent retreat history: a review, *Quat. Sci. Rev.*, *21*, 49-70

Andreassen, K. and M. Winsborrow (2009), Signature of ice streaming in Bjørnøyrenna, Polar North Atlantic, through the Pleistocene and implications for ice-stream dynamics. *Annals of Glaciology*, 50, 17-26.

Arthern, R.J., R.C.A. Hindmarsh, and C.R. Williams (2015), Flow speed within the Antarctic ice sheet and its controls inferred from satellite observations. J. Geophys. Res. Earth Surf., 120, 1171–1188

Atkinson, N., D.J. Utting, and S.M. Pawley (2014), Landform signature of the Laurentide and Cordilleran ice sheets across Alberta during the last glaciation. *Can. J. Earth Sci., 51*, 1067-1083.

Baas, A.C.W. (2002), Chaos, fractals and self-organization in coastal geomorphology: Simulating dune landscapes in vegetated environments, *Geomorphology*, *48*, 309-328.

Bamber, J.L., D.G. Vaughan and I. Joughin (2000), Widespread complex flow in the interior of the Antarctic ice sheet, *Science, 287,* 1248-1250.

Barchyn, T.E., T.P.F. Dowling, C.R. Stokes, and C.H. Hugenholtz (2016), Subglacial bed form morphology controlled by ice speed and sediment thickness, *Geophys. Res. Lett., 43*, 7572–7580, doi:10.1002/ 2016GL069558.

Beget, J.E. (1986), Modeling the Influence of Till Rheology on the Flow and Profile of the Lake Michigan Lobe, Southern Laurentide Ice Sheet, U.S.A. *J. Glaciol., 32*, 235-241.

Bennett, M.R. (2003), Ice streams as the arteries of an ice sheet: their mechanics, stability and significance. *Earth-Sci. Rev.*, 61, 309–339.

Bingham, R.G. and M.J. Siegert (2009), Quantifying subglacial bed roughness in Antarctica: implications for ice-sheet dynamics and history. *Quat. Sci. Rev.*, 28, 223–236

772 Bindschadler, R.A., M.A. King, R.B. Alley, S. Anandakrishnan and L. Padman (2003),
773 Tidally controlled stick-slip discharge of a West Antarctic Ice Stream, *Science*, 301,
774 1087–1089.
775 Bluemle, J.P., M.L. Lord and N.T. Hunke (1993), Exceptionally long, narrow drumlins
776 formed in subglacial cavities, North Dakota. *Boreas*, 22, 15-24.
777 Boulton, G.S. (1987), A theory of drumlin formation by subglacial sediment deformation. In:
778 Menzies, J., Rose, J. (Eds.), Drumlin Symposium. A.A. Balkema, Rotterdam, pp. 25-80
779 Brown, S.R. and C.H. Scholz (1985), Broad bandwidth study of the topography of natural
780 rock surfaces. *Journal of Geophysical Research*, 90, 12,575-12,582.
781 Canals, M., R. Urgeles, and A.M. Calafat (2000), Deep sea floor evidence of past ice streams
782 off the Antarctic Peninsula. *Geology, 28,* 31-34.
783 Clark C.D. (1993). Mega-scale glacial lineations and cross-cutting iceflow landforms. *Earth*
784 *Surf. Processes Landforms, 18*, 1–29.
785 Clark, C.D. (1994), Large-scale ice-moulding: a discussion of genesis and glaciological
786 significance, *Sediment. Geol.*, *91*(1), 253–268.
787 Clark, C.D., S.M. Tulaczyk, C.R. Stokes and M. Canals (2003), A groove-ploughing theory
788 for the production of mega-scale glacial lineations, and implications for ice-stream
789 mechanics. *J. Glaciol. 49,* 240–256.
790 Dowdeswell, J.A., C. Ó Cofaigh and C.J. Pudsey (2004), Thickness and extent of the
791 subglacial till layer beneath an Antarctic paleo-ice stream. *Geology, 32,* 13-16.
792 Dowdeswell, J.A., D. Ottesen and L. Rise (2006), Flow-switching and large-scale deposition
793 by ice streams draining former ice sheets. *Geology, 34,* 313-316.
794 Dowdeswell, J.A., D. Ottesen, J. Evans, C. Ó Cofaigh and J.B. Anderson (2008), Submarine
795 glacial landforms and rates of ice-stream collapse. *Geology, 36*, 819-822.
796 Dowdeswell, E.K., B.J. Todd and J.A. Dowdeswell, (2016), Crag-and-tail features:
797 convergent ice flow through Eclipse Sound, Baffin Island, Arctic Canada. In
798 Dowdeswell, J.A. et al., (eds), *Atlas of Submarine Glacial Landforms: Modern,*
799 *Quaternary and Ancient.* Geological Society, London, Memoirs, 46, 55-56.
800 Ely, J.C., C.D. Clark, M. Spagnolo, C.R. Stokes, S.L. Greenwood, A.L.C. Hughes, P. Dunlop
801 and D. Hess (2016), Do subglacial bedforms comprise a size and shape continuum?
802 *Geomorphology, 257,* 108-119.

803 Engelhardt, H., N. Humphrey, B. Kamb and M. Fahnestock (1990), Physical conditions at the
804 base of a fast moving Antarctic ice stream. *Science*, 248(4951), 57-59.
805 Finlayson, A. (2013) Digital surface models are not always representative of former glacier
806 beds: palaeoglaciological and geomorphological implications, *Geomorphology, 194*,
807 25–33.
808 Fisher, A.T., K.D. Mankoff, S.M. Tulaczyk, S.W. Tyler, N. Foley and the WISSARD
809 Science Team (2015), High geothermal heat flux measured below the West Antarctic
810 Ice Sheet. *Science Advances*, 1, 6, e1500093
811 Fourrière, A., P. Claudin, and B. Andreotti (2010), Bedforms in a turbulent stream:
812 Formation of ripples by primary linear instability and of dunes by nonlinear pattern
813 coarsening, *J. Fluid Mech., 649,* 287-328.
814 Fowahuh, G.F. and C.D. Clark (1995), Geomorphic analysis of aeolian and glacial linear
815 features using satellite imagery. *Proceedings of the 21st Annual conference of the*
816 *Remote Sensing Society,* Southampton, 858-865.
817 Fowler, A.C. (2010), The formation of subglacial streams and mega-scale glacial lineations,
818 *Proceedings of the Royal Society of London A: Mathematical, Physical and*
819 *Engineering Sciences*, 466, 3181–3201.
820 Fowler, A. C., and M. Chapwanya (2014), An instability theory for the formation of ribbed
821 moraine, drumlins and mega-scale glacial lineations, *Proc. Royal Soc. A*, 470,
822 20140185
823 Gales, J.A., R.D. Larter, N.C. Mitchell and J.A. Dowdeswell (2013), Geomorphic signature
824 of Antarctic submarine gullies: implications for continental slope processes, *Marine*
825 *Geology*, 337, 112–124
826 Graham, A.G.C., L. Lonergan and M.S. Stoker (2007), Evidence for Late Pleistocene ice
827 stream activity in the Witch Ground Basin, central North Sea, from 3D seismic
828 reflection data. *Quat. Sci. Rev.*, 26, 627-643.
829 Hallet B. (1990) Spatial self-organization in geomorphology: from periodic bedforms and
830 patterned ground to scale-invariant topography. *Earth-Sci. Rev., 29*, 57–75
831 Hicock, S.R., F.J. Kristjansson, and D.R. Sharpe (1989), Carbonate till as a soft bed for
832 Pleistocene ice streams on the Canadian Shield north of Lake Superior, *Can. J. Earth*
833 *Sci.*, *26*, 2249–2254.
834 Hindmarsh, RCA. (1999), Coupled ice-till dynamics and the seeding of drumlins and bedrock
835 forms. *Ann. Glaciol.*, 28, 221–230.

836 Jakobsson M., J.B. Anderson, F.O. Nitsche, J.A. Dowdeswell, R. Gyllencreutz, N. Kirchner,
837 M.A. O'Regan, R.B. Alley, S. Anandakrishnan, R. Mohammad, B. Eriksson, R.
838 Fernandez, A. Kirshner, R. Minzoni, T. Stolldorf and W. Majewski (2011), Geological
839 record of Ice Shelf Breakup and Grounding Line Retreat, Pine Island Bay, West
840 Antarctica. *Geology*, 39, 691-694.

841 Jamieson, S.R., A. Vieli, C. Ó Cofaigh, C.R. Stokes, S.J. Livingstone and C.-D. Hillenbrand
842 (2014), Understanding controls on rapid ice-stream retreat during the last deglaciation
843 of Marguerite Bay, Antarctica, using a numerical model. *J. Geophys. Res.: Earth*
844 *Surface*, 119, 247-263.

845 Jamieson, S.R., C.R. Stokes, S.J. Livingstone, A. Vieli, C. Ó Cofaigh, C.-D. Hillenbrand and
846 M. Spagnolo (2016), Subglacial processes on an Antarctic Ice Stream bed 2: Can
847 modelled ice dynamics explain the morphology of mega-scale glacial lineations?
848 *Journal of Glaciology*, 62, 232, 285-298

849 Joughin, D.R., S. MacAyeal and S. Tulaczyk (2004), Basal shear stress of the Ross ice
850 streams from control method inversions. *J. Geophys. Res.*, 109

851 King, E.C., R.C.A. Hindmarsh and C.R. Stokes (2009), Formation of mega-scale glacial
852 lineations observed beneath a West Antarctic ice stream, *Nat. Geosci.*, *2*(8), 585–588.

853 King, E.C., H.D. Pritchard and A.M. Smith (2016), Subglacial landforms beneath Rutford Ice
854 Stream, Antarctica: detailed bed topography from ice-penetrating radar, *Earth Syst. Sci.*
855 *Data, 8*, 151-158.

856 Krabbendam, M. and T. Bradwell (2011), Lateral plucking as a mechanism for elongate
857 erosional glacial bedforms: explaining megagrooves in Britain and Canada. *Earth Surf.*
858 *Processes Landforms*, 36, 335-1349.

859 Larter, R.D., A.G.C. Graham, K. Gohl, G. Kuhn, C.-D. Hillenbrand, J.A. Smith, T.J. Deen,
860 R.A. Livermore and H.W. Schenke (2009), Subglacial bedforms reveal complex basal
861 regime in a zone of paleo–ice stream convergence, Amundsen Sea embayment, West
862 Antarctica, *Geology*, *37*, 411–414.

863 Lemke, R.W. (1958), Narrow linear drumlins near Velva, North Dakota. *Am. J. Sci.*, 256,
864 270-283.

865 Li, X., B. Sun, M.J. Siegert, R.G. Bingham, X. Tang, D. Zhang, X. Cui and X. Zhang (2010),
866 Characterization of subglacial landscapes by a two-parameter roughness index. *J.*
867 *Glaciol.*, 56, 831-836.

868 Livingstone, S.J., C. Ó Cofaigh, C.R. Stokes, C.D. Hillenbrand, A. Vieli and S.S.R. Jamieson
869 (2013), Glacial geomorphology of Marguerite Bay Palaeo-Ice Stream, western
870 Antarctica Peninsula. *J. Maps*, 9, 558–572.
871 Livingstone, S.J., C. Ó Cofaigh, K.A. Hogan and J.A. Dowdeswell (2016a), Submarine
872 glacial-landform distribution along an Antarctic Peninsula palaeo-ice stream: a shelf-
873 slope transect through the Marguerite Bay system (66 to 70°S). In Dowdeswell, J.A. et
874 al., (eds), *Atlas of Submarine Glacial Landforms: Modern, Quaternary and Ancient*.
875 Geological Society, London, Memoirs, v. 46, p. 485-492.
876 Livingstone, S.J., C.R. Stokes, C.D. Hillenbrand, A. Vieli, S.S.R. Jamieson, M. Spagnolo and
877 J.A. Dowdeswell (2016b), Subglacial processes on an Antarctic ice stream bed. 1:
878 Sediment transport and bedform genesis inferred from marine geophysical data. *J.*
879 *Glaciol.*, *62,* 270-284.
880 Mandelbrot, B.B. (1982), The Fractal Geometry of Nature. W.H. Freeman, San Francisco,
881 Calif., 461 pp.
882 Margold, M., C.R. Stokes and C.D. Clark (2015a), Ice streams in the Laurentide Ice Sheet:
883 Identification, characteristics and comparison to modern ice sheets, *Earth-Sci. Rev.*,
884 *143*, 117–146.
885 Margold, M., C.R. Stokes, C.D. Clark and J. Kleman (2015b), Ice streams in the Laurentide
886 Ice Sheet: a new mapping inventory, *J. Maps*, *11*(3), 380–395.
887 Ó Cofaigh, C., C.J. Pudsey, J.A. Dowdeswell and P. Morris (2002), Evolution of subglacial
888 bedforms along a paleo-ice stream, Antarctic Peninsula continental shelf. *Geophys. Res.*
889 *Letters*, *29*, 41, 1-4.
890 Ó Cofaigh C., J.A. Dowdeswell, C.S. Allen, J.F. Hiemstra, C.J. Pudsey, J. Evans and D.J.A.
891 Evans (2005), Flow dynamics and till genesis associated with a marine-based Antarctic
892 palaeo-ice stream. *Quat. Sci. Rev., 24*, 709–740.
893 Ó Cofaigh, C., C.R. Stokes, O.B. Lian, C.D. Clark and S. Tulacyzk (2013), Formation of
894 mega-scale glacial lineations on the Dubawnt Lake Ice Stream bed: 2. Sedimentology
895 and stratigraphy, *Quat. Sci. Rev.*, *77*, 210–227.
896 Perron, J.T., J.W. Kirchner and W.E. Dietrich (2008), Spectral signatures of characteristic
897 spatial scales and nonfractal structure in landscapes. *J. Geophys. Res., 113,* F04003
898 Piasecka, E.D., M.C.M. Winsborrow, K. Andreassen and C.R. Stokes (2016) Reconstructing
899 the retreat dynamics of the Bjørnøyrenna Ice Stream based on new 3D seismic data
900 from the central Barents Sea. *Quat. Sci. Rev.*, 151, 212-227.

Piotrowski, J.A., N.K. Larsen and F.W. Junge (2004), Reflections on soft subglacial beds as a mosaic of deforming and stable spots. *Quat. Sci. Rev., 23,* 993–1000.

Rignot, E. and Kanagaratnam, P. (2006) Changes in the velocity structure of the Greenland Ice Sheet. *Science, 311*, 986-988.

Rignot, E., J. Mouginot, and B. Scheuchl (2011), Ice flow of the Antarctic ice sheet. *Science*, 333, 1427-1430.

Rippin, D.M., R.G. Bingham, T.A. Jordan, A.P. Wright, N. Ross, H.F.J. Corr, F. Ferraccioli, A.M. Le Brocq, K.C. Rose and M.J. Siegert (2014), Basal roughness of the Institute and Möller Ice Streams, West Antarctica: Process determination and landscape interpretation, *Geomorphology, 214,* 139-147.

Sayles, R.S. and T.R. Thomas (1978), Surface topography as a non-stationary random process. *Nature*, 271, 431-434.

Schoof, C. (2002), Basal perturbations under ice streams: form drag and surface expression. *J. Glaciol*., 48, 407-416

Schoof, C. (2007), Pressure-dependent viscosity and interfacial instability in coupled ice-sediment flow. *J. Fluid Mech*. *570*, 227-252.

Shaw, J., A. Pugin and R.R. Young (2008), A meltwater origin for Antarctic shelf bedforms with special attention to megalineations, *Geomorphology, 102*(3–4), 364–375.

Smith, A.M., T. Murray, K.W. Nicholls, K. Makinson, G. Aðalgeirsdóttir, A.E. Behar and D. G. Vaughan (2007), Rapid erosion, drumlin formation, and changing hydrology beneath an Antarctic ice stream, *Geology*, *35*(2), 127–130.

Smith, A.M., T.A. Jordan, F. Ferraccioli and R.G. Bingham (2013), Influence of subglacial conditions on ice stream dynamics: Seismic and potential field data from Pine Island Glacier, West Antarctica, *J. Geophys. Res. Solid Earth*, 118, 1471–1482

Spagnolo, M., C.D. Clark, J.C. Ely, C.R. Stokes, J.B. Anderson, K. Andreassen, A.G.C. Graham and E.C. King (2014a), Size, shape and spatial arrangement of mega-scale glacial lineations from a large and diverse dataset, *Earth Surf. Processes Landforms*, *39*(11), 1432–1448.

Spagnolo M., E. Philips, J.A. Piotrowski, B.R. Rea, C.D. Clark, C.R. Stokes, J. Carr, J.C. Ely, A. Ribolini, W. Wysota and I. Szuman (2016). Ice stream motion facilitated by a shallow-deforming and accreting bed. *Nat. Commun.*, *7*, 10723.

Stokes, C.R., and C.D. Clark (2001), Palaeo-ice streams, *Quat. Sci. Rev.*, *20*, 1437–1457.

Stokes, C.R., M. Spagnolo, C.D. Clark, C. Ó Cofaigh, O.B. Lian and R. B. Dunstone (2013), Formation of mega-scale glacial lineations on the Dubawnt Lake Ice Stream bed: 1.

size, shape and spacing from a large remote sensing dataset, *Quat. Sci. Rev.*, *77*, 190–209.

Stokes, C.R., M. Margold, C.D. Clark and L. Tarasov (2016), Ice stream activity scaled to ice sheet volume during Laurentide Ice Sheet deglaciation, *Nature*, *530*(7590), 322–326.

Tulaczyk, S.M., R.P. Scherer and C.D. Clark (2001), A ploughing model for the origin of weak tills beneath ice streams: a qualitative treatment, *Quat. Int.*, *86*(1), 59–70.

Wellner, J.S., A.L. Lowe, S.S. Shipp and J.B. Anderson (2001), Distribution of glacial geomorphic features on the Antarctic continental shelf and correlation with substrate: implications for ice behaviour. *J. Glaciol.*, 47, 397-411.

Woodworth-Lynas, C.M.T., H.W. Josenhans, J.V. Barrie, C.F.M. Lewis and D.R. Parrott, (1991), The physical processes of seabed disturbance during iceberg grounding and scouring. *Continental Shelf Research*, **11**, 939-951.

Region	Resolution		Name	Figure	Setting	Activity	Morphology	Area	Mid point		Dominant	Dominant	Max normalized
	horizontal	vertical						km^2	latitude	longitude	orientation (°)	wavelength (m)	amplitude
Amundsen Sea Embayment, Antarctica	30 m	2 m	ASE_bedrock_1	1a	marine	paleo	streamlined bedrock	100	73.618 S	115.276 W	30.2	1327	8
Amundsen Sea Embayment, Antarctica	30 m	2 m	ASE_bedrock_2	1a	marine	paleo	crag and tails	100	73.524 S	115.202 W	22.6	282	5
Amundsen Sea Embayment, Antarctica	30 m	2 m	ASE_MSGL_1	1a	marine	paleo	MSGLs	100	73.430 S	115.230 W	-13	1188	14
Amundsen Sea Embayment, Antarctica	30 m	2 m	ASE_MSGL_2	1a	marine	paleo	MSGLs	100	73.335 S	115.254 W	-16.2	332	15
Amundsen Sea Embayment, Antarctica	30 m	2 m	ASE_MSGL_3	1a	marine	paleo	MSGLs	100	73.241 S	115.321 W	-30.8	600	13
Pine Island, Antarctica	20 m	1 m	PI_furrows	1b	marine	paleo	iceberg furrows	100	72.929 S	107.152 W	-11.6	1992	4
Pine Island, Antarctica	20 m	1 m	PI_MSGL_1	1b	marine	paleo	MSGLs	100	73.264 S	107.015 W	-12.6	689	42
Pine Island, Antarctica	20 m	1 m	PI_MSGL_2	1b	marine	paleo	MSGLs	100	72.743 S	107.207 W	-18.4	348	34
Lower Athabasca region, Alberta, Canada	2 m	0.1 m	LAR_MSGL	1c	terrestrial	paleo	MSGLs	100	57.865 N	111.989 W	55.8	1626	4
Lower Athabasca region, Alberta, Canada	2 m	0.1 m	LAR_fluvial	1c	terrestrial	paleo	fluvial landscape	100	57.887 N	112.179 W	-86.2	1973	2
Lower Athabasca region, Alberta, Canada	2 m	0.1 m	LAR_flat	1c	terrestrial	paleo	fluvial terrace	100	57.833 N	111.692 W	33.8	1992	2
Marguerite Trough, Antarctica	15 m	1 m	MT_gullies	1d	marine	paleo	shelf break gullies	100	66.551 S	71.694 W	119.8	763	6
Marguerite Trough, Antarctica	15 m	1 m	MT_furrows	1d	marine	paleo	iceberg furrows	100	66.486 S	71.276 W	148.4	1992	4
Marguerite Trough, Antarctica	15 m	1 m	MT_MSGL_1	1d	marine	paleo	MSGLs	100	66.735 S	70.662 W	142	749	17
Marguerite Trough, Antarctica	15 m	1 m	MT_MSGL_2	1d	marine	paleo	MSGLs	100	66.535 S	70.964 W	131.4	317	11
Marguerite Trough, Antarctica	15 m	1 m	MT_MSGL_3	1d	marine	paleo	MSGLs	100	66.866 S	70.860 W	128.6	791	7
Marguerite Trough, Antarctica	15 m	1 m	MT_bedrock_1	1f	marine	paleo	bedrock	100	68.696 S	69.638 W	105.6	1232	6
Marguerite Trough, Antarctica	15 m	1 m	MT_bedrock_2	1f	marine	paleo	bedrock	100	67.965 S	70.340 W	15.4	1390	7
Marguerite Trough, Antarctica	15 m	1 m	MT_bedrock_3	1f	marine	paleo	bedrock	100	68.248 S	69.920 W	3	943	6
Rutford Ice Stream, Antarctica	7.5-500 m	3 m	RIS_MSGL_1	1e	marine	current	MSGLs	100	78.425 S	84.048 W	158	329	N/A
Rutford Ice Stream, Antarctica	7.5-500 m	3 m	RIS_MSGL_2	1e	marine	current	MSGLs	100	78.523 S	83.774 W	160	504	N/A
Rutford Ice Stream, Antarctica	7.5-500 m	3 m	RIS_MSGL_3	1e	marine	current	MSGLs	100	78.619 S	83.496 W	159.8	361	N/A

Figure 1.

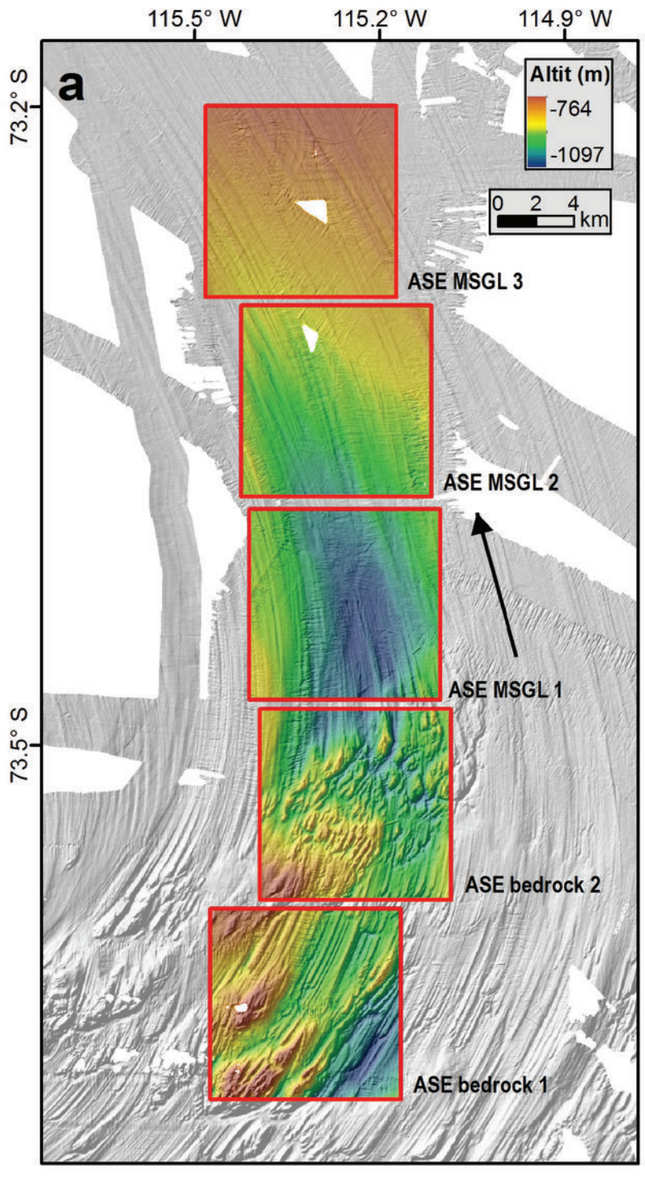
a
115.5° W
115.2° W
114.9° W
73.2° S
73.5° S
Altit (m)
-764
-1097
0 2 4 km
ASE MSGL 3
ASE MSGL 2
ASE MSGL 1
ASE bedrock 2
ASE bedrock 1

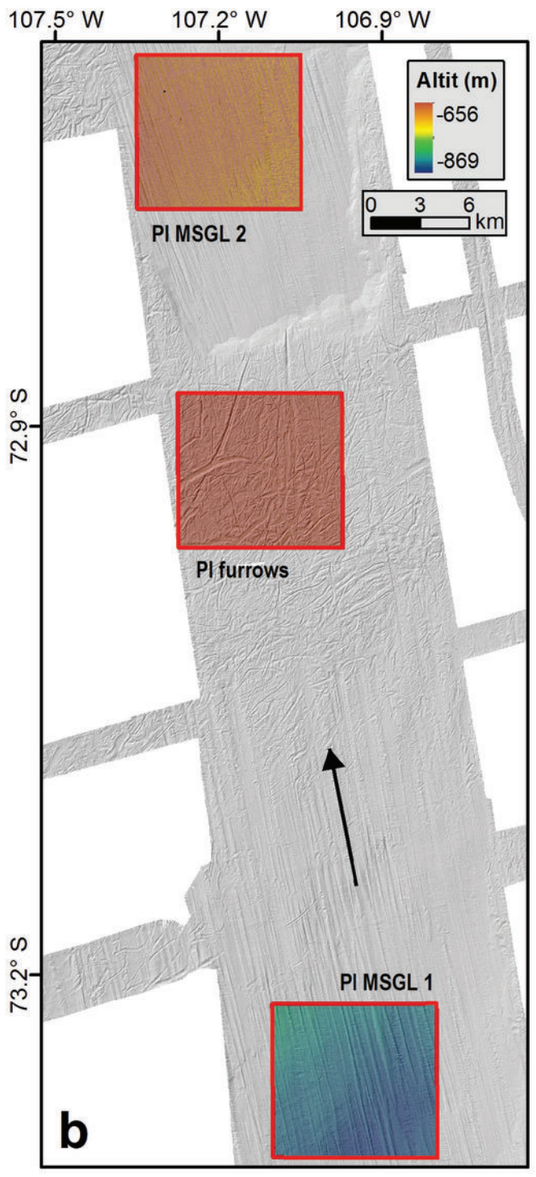
b
107.5° W
107.2° W
106.9° W
72.9° S
73.2° S
Altit (m)
-656
-869
0 3 6 km
PI MSGL 2
PI furrows
PI MSGL 1

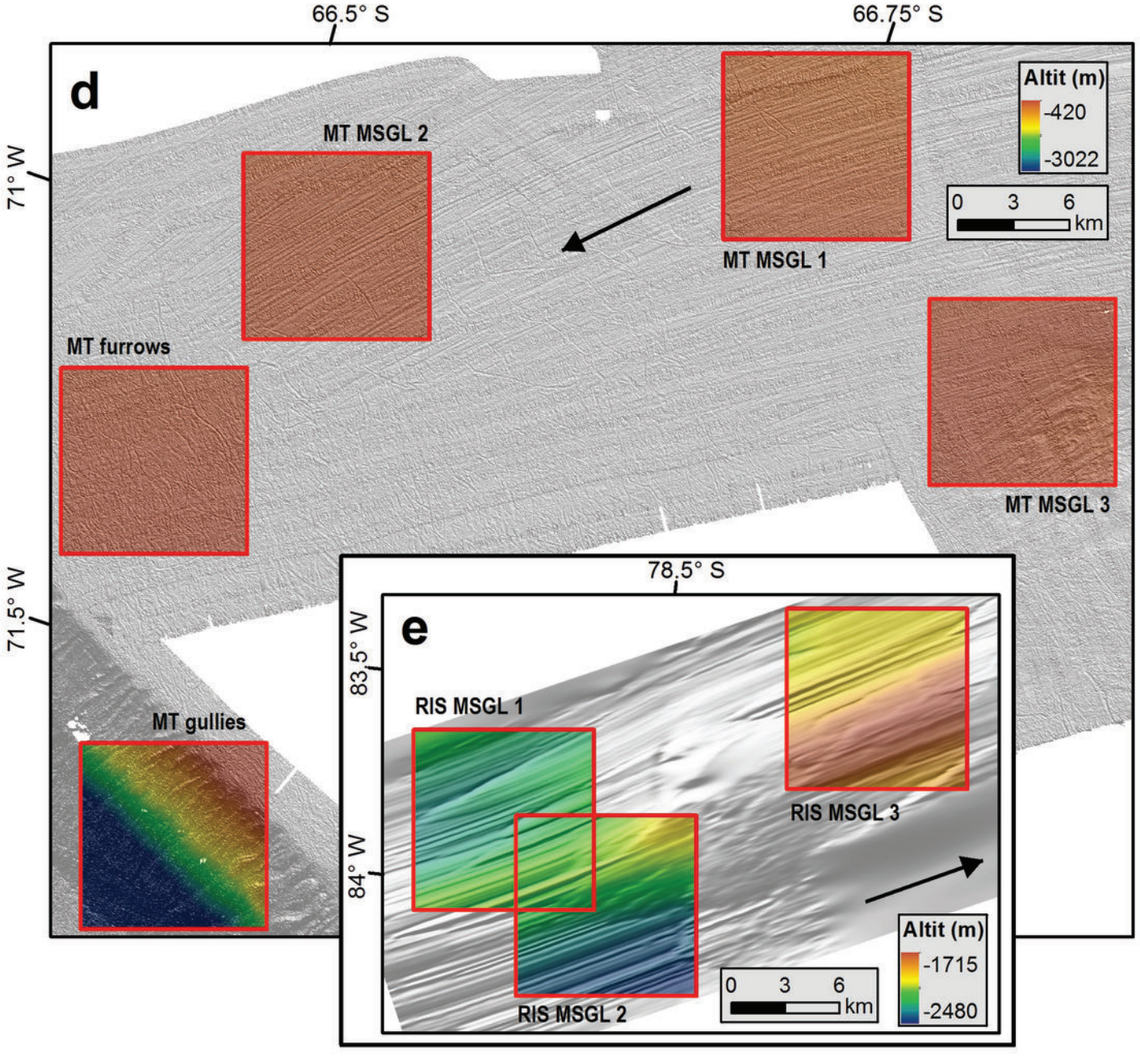
d
66.5° S
66.75° S
71° W
71.5° W
Altit (m)
-420
-3022
0 3 6 km
MT MSGL 2
MT MSGL 1
MT furrows
MT MSGL 3
MT gullies

e
78.5° S
83.5° W
84° W
RIS MSGL 1
RIS MSGL 3
RIS MSGL 2
Altit (m)
-1715
-2480
0 3 6 km

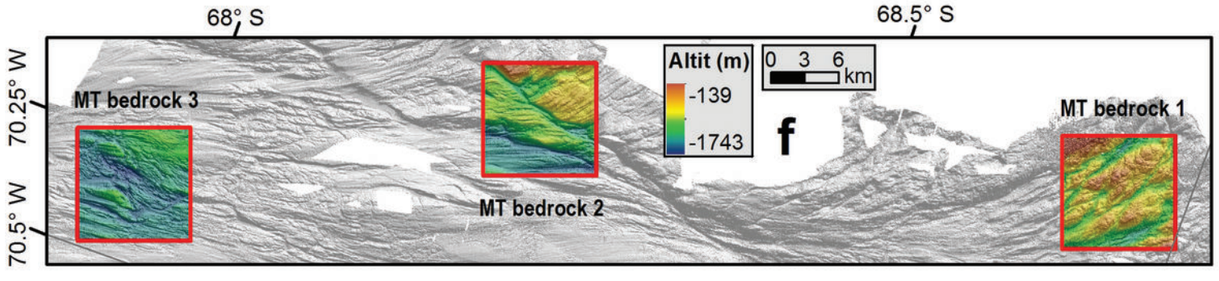
68° S
68.5° S
70.25° W
70.5° W
Altit (m)
-139
-1743
0 3 6 km
f
MT bedrock 3
MT bedrock 2
MT bedrock 1

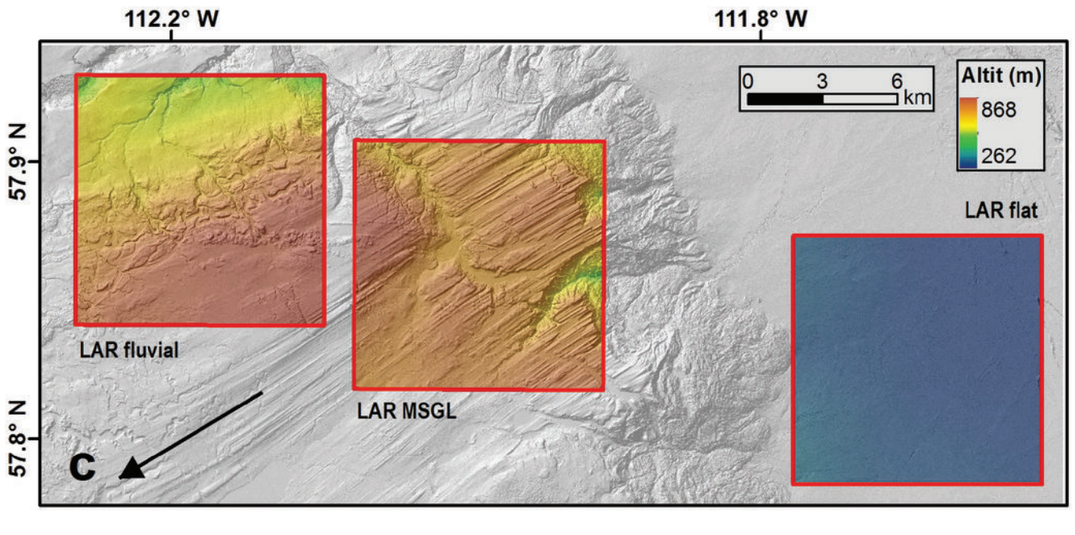
112.2° W
111.8° W
57.9° N
57.8° N
0 3 6 km
Altit (m)
868
262
LAR flat
LAR fluvial
LAR MSGL
c

Figure 2.

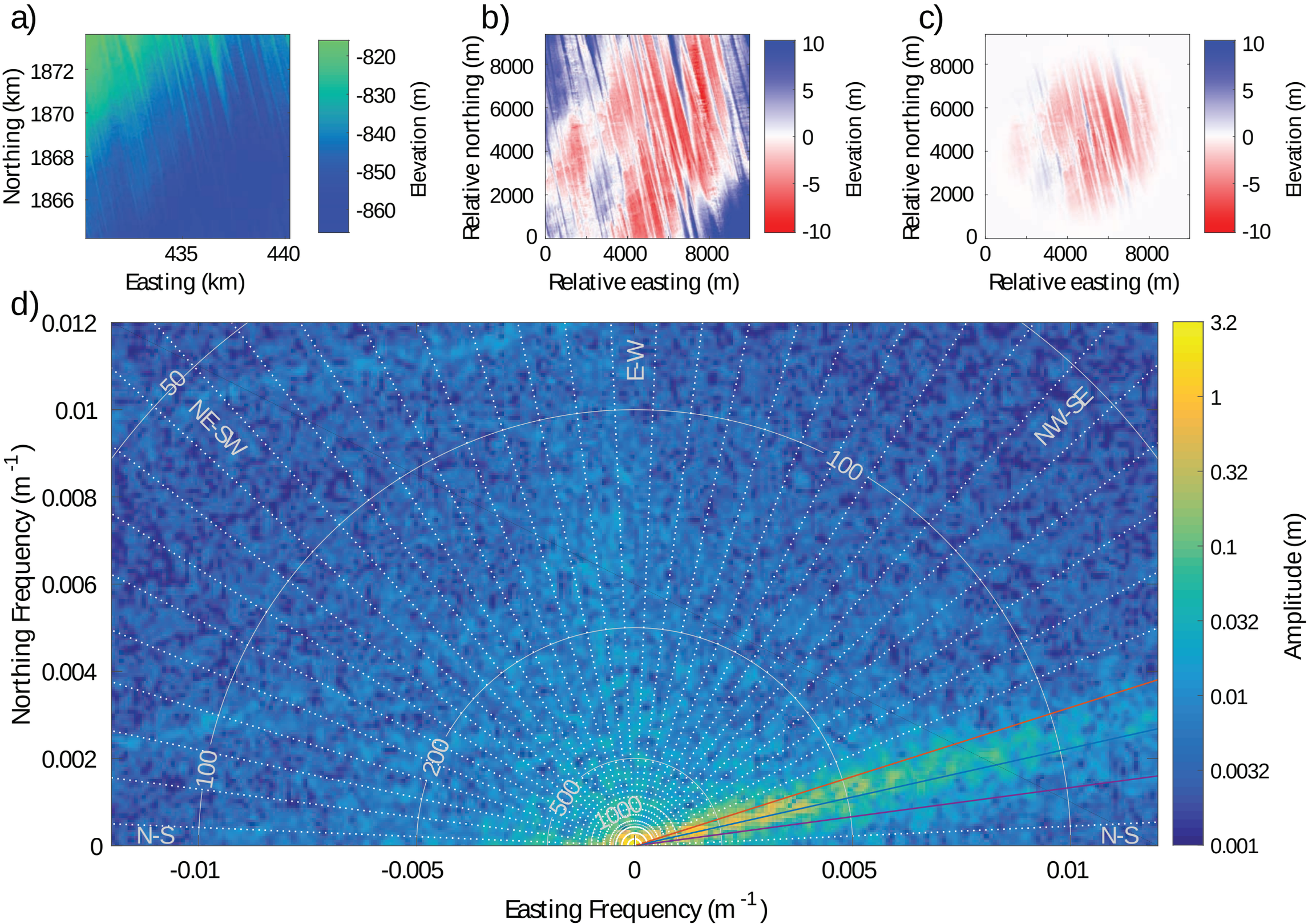
a)
Northing (km)
1872
1870
1868
1866
435
440
Easting (km)
-820
-830
-840
-850
-860
Elevation (m)
b)
Relative northing (m)
8000
6000
4000
2000
0
0
4000
8000
Relative easting (m)
10
5
0
-5
-10
Elevation (m)
c)
Relative northing (m)
8000
6000
4000
2000
0
0
4000
8000
Relative easting (m)
10
5
0
-5
-10
Elevation (m)
d)
Northing Frequency (m -1)
0.012
0.01
0.008
0.006
0.004
0.002
0
-0.01
-0.005
0
0.005
0.01
Easting Frequency (m -1)
50
NE-SW
E-W
NW-SE
100
100
200
500
1000
N-S
N-S
3.2
1
0.32
0.1
0.032
0.01
0.0032
0.001
Amplitude (m)

Figure 3.

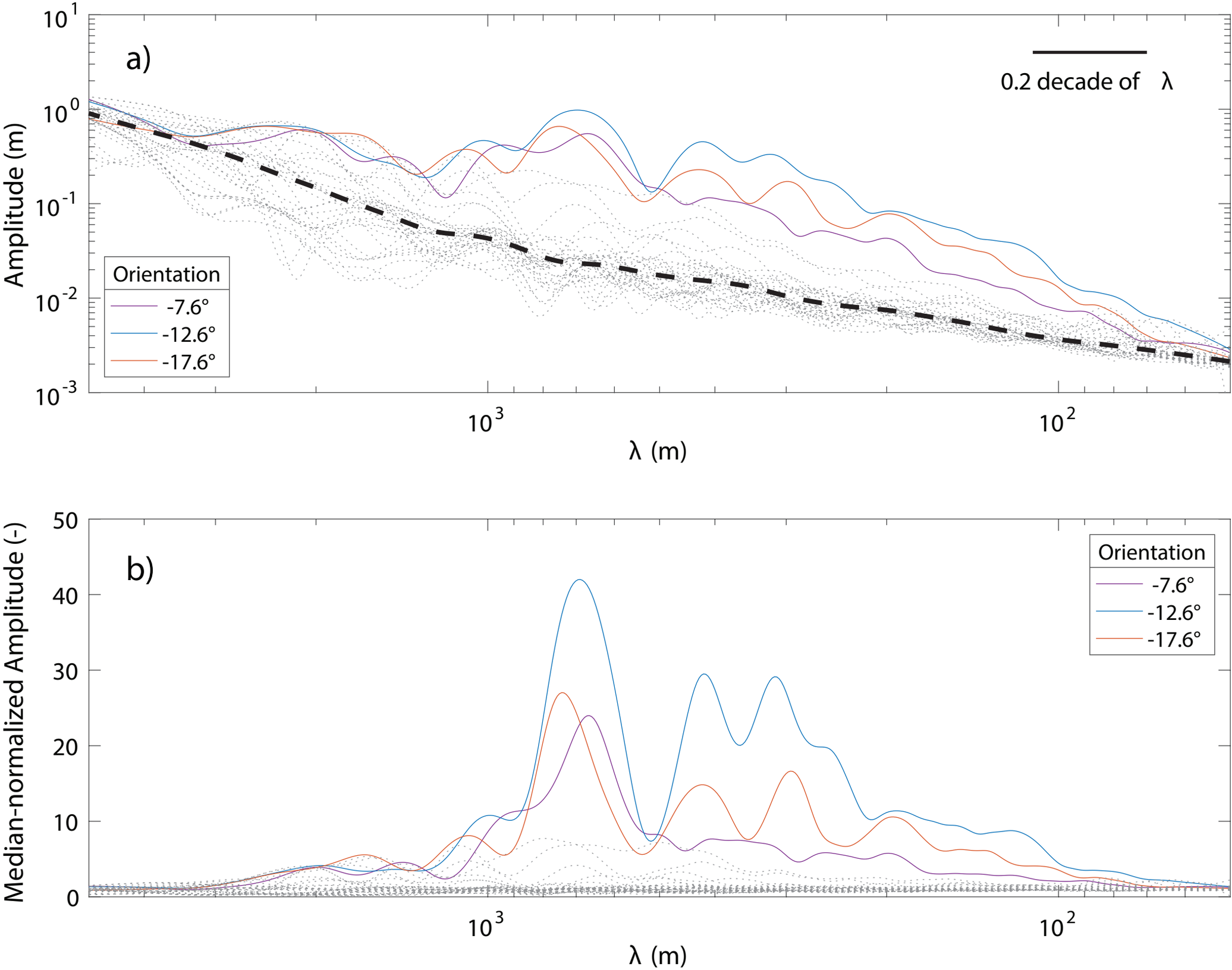
a)
0.2 decade of λ
Amplitude (m)
10^{1}
10^{0}
10^{-1}
10^{-2}
10^{-3}
Orientation
-7.6°
-12.6°
-17.6°
10^{3}
10^{2}
λ (m)
b)
Median-normalized Amplitude (-)
50
40
30
20
10
0
Orientation
-7.6°
-12.6°
-17.6°
10^{3}
10^{2}
λ (m)

Figure 4.

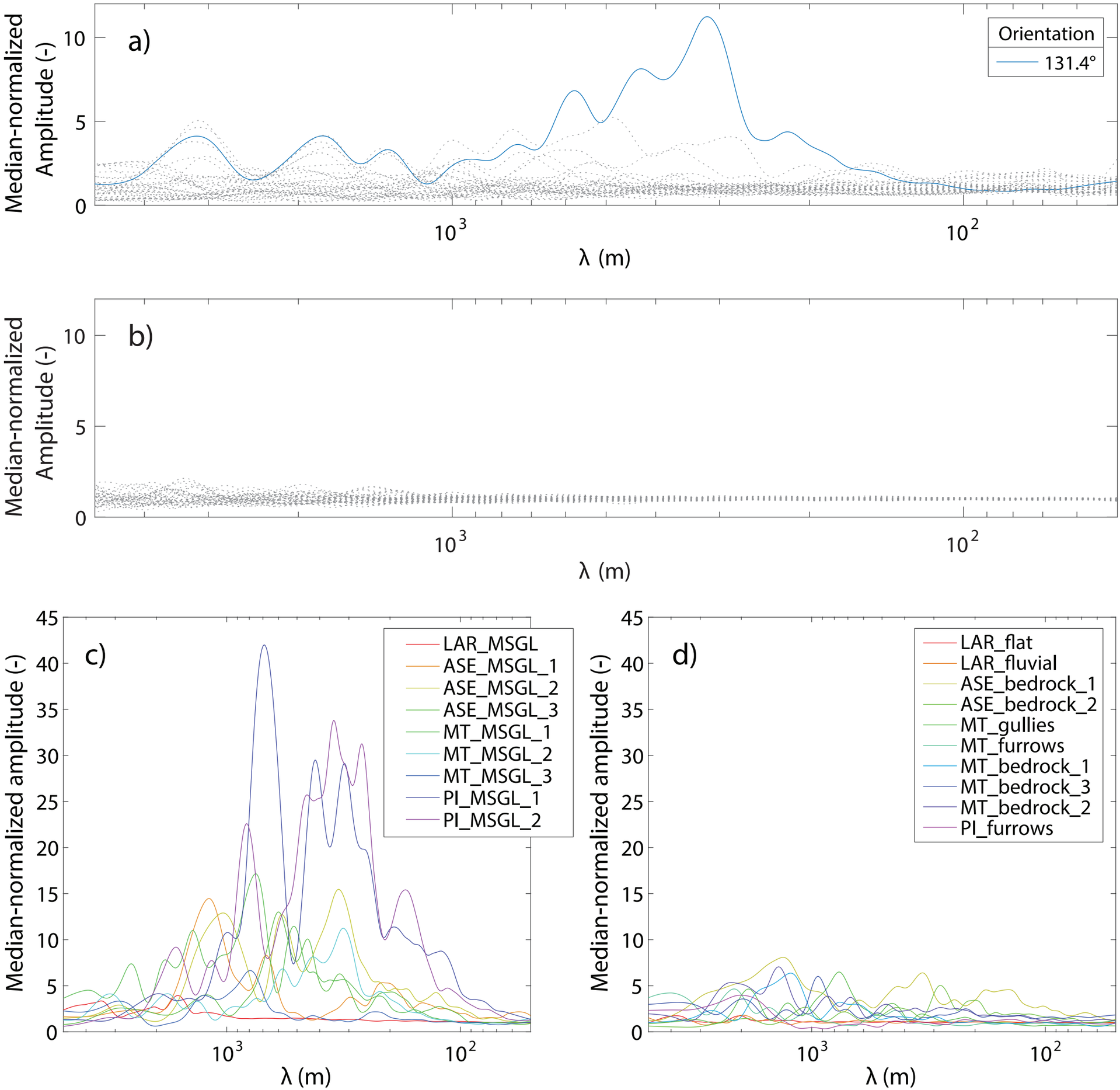
a)
Median-normalized Amplitude (-)
Orientation
131.4°
λ (m)
b)
c)
LAR_MSGL
ASE_MSGL_1
ASE_MSGL_2
ASE_MSGL_3
MT_MSGL_1
MT_MSGL_2
MT_MSGL_3
PI_MSGL_1
PI_MSGL_2
Median-normalized amplitude (-)
d)
LAR_flat
LAR_fluvial
ASE_bedrock_1
ASE_bedrock_2
MT_gullies
MT_furrows
MT_bedrock_1
MT_bedrock_3
MT_bedrock_2
PI_furrows

Figure 5.

a)

b = 1.5

b = 2.3

b = 0.5

Amplitude (m)

λ (m)

LAR_□at
LAR_□uvial
ASE_bedrock_1
ASE_bedrock_2
MT_gullies
MT_furrows
MT_bedrock_1
MT_bedrock_3
MT_bedrock_2
PI_furrows

b)

b = 1.5

b = 2.3

b = 0.5

Amplitude (m)

λ (m)

LAR_MSGL
ASE_MSGL_1
ASE_MSGL_2
ASE_MSGL_3
MT_MSGL_1
MT_MSGL_2
MT_MSGL_3
PI_MSGL_1
PI_MSGL_2

c)

b = 1.5

b = 2.3

b = 0.5

Amplitude (m)

λ (m)

LAR_MSGL
ASE_MSGL_1
ASE_MSGL_2
ASE_MSGL_3
MT_MSGL_1
MT_MSGL_2
MT_MSGL_3
PI_MSGL_1
PI_MSGL_2
RIS_MSGL_1
RIS_MSGL_2
RIS_MSGL_3

Figure 6.

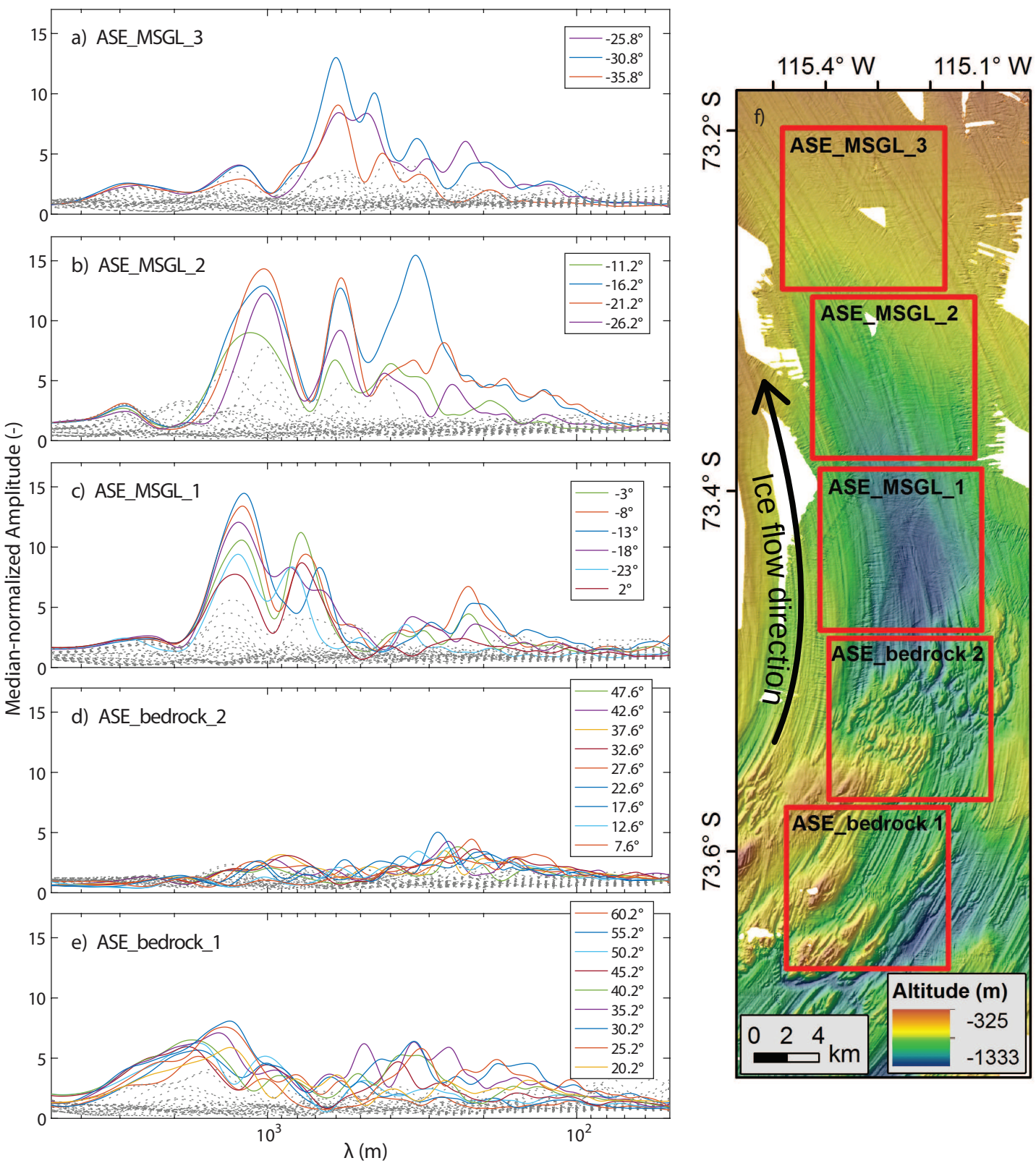
a) ASE_MSGL_3
-25.8°
-30.8°
-35.8°
b) ASE_MSGL_2
-11.2°
-16.2°
-21.2°
-26.2°
c) ASE_MSGL_1
-3°
-8°
-13°
-18°
-23°
2°
d) ASE_bedrock_2
47.6°
42.6°
37.6°
32.6°
27.6°
22.6°
17.6°
12.6°
7.6°
e) ASE_bedrock_1
60.2°
55.2°
50.2°
45.2°
40.2°
35.2°
30.2°
25.2°
20.2°
Median-normalized Amplitude (-)
λ (m)
10^3
10^2
f)
115.4° W
115.1° W
73.2° S
73.4° S
73.6° S
ASE_MSGL_3
ASE_MSGL_2
ASE_MSGL_1
ASE_bedrock 2
ASE_bedrock 1
Ice flow direction
Altitude (m)
-325
-1333
0 2 4
km

Figure 7.

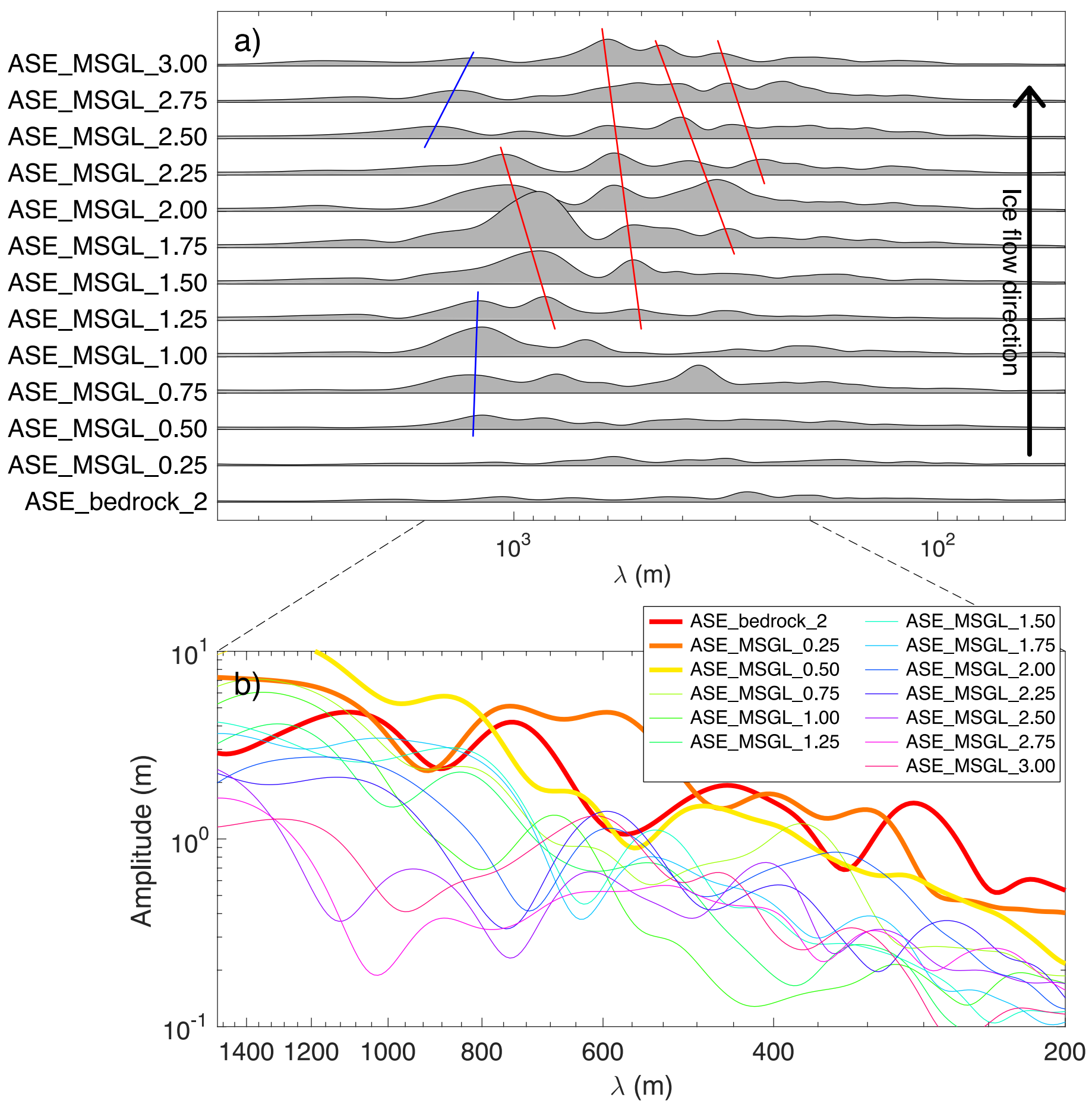
a)
ASE_MSGL_3.00
ASE_MSGL_2.75
ASE_MSGL_2.50
ASE_MSGL_2.25
ASE_MSGL_2.00
ASE_MSGL_1.75
ASE_MSGL_1.50
ASE_MSGL_1.25
ASE_MSGL_1.00
ASE_MSGL_0.75
ASE_MSGL_0.50
ASE_MSGL_0.25
ASE_bedrock_2
Ice flow direction
10^3
10^2
λ (m)
b)
ASE_bedrock_2
ASE_MSGL_0.25
ASE_MSGL_0.50
ASE_MSGL_0.75
ASE_MSGL_1.00
ASE_MSGL_1.25
ASE_MSGL_1.50
ASE_MSGL_1.75
ASE_MSGL_2.00
ASE_MSGL_2.25
ASE_MSGL_2.50
ASE_MSGL_2.75
ASE_MSGL_3.00
Amplitude (m)
10^1
10^0
10^{-1}
1400 1200 1000 800 600 400 200
λ (m)